Efficacy and mechanism of action of cipargamin as an antibabesial drug candidate

Authors

Hang Li[1#], Shengwei Ji[1,2#], Nanang R. Ariefta[1], Eloiza May S. Galon[3], Shimaa AES El-Sayed[1,4], Thom Do[1], Lijun Jia[2], Miako Sakaguchi[5], Masahito Asada[1], Yoshifumi Nishikawa[1], Xin Qin[6], Mingming Liu[6]*, Xuenan Xuan[1,7]*

Affiliations

[1]National Research Center for Protozoan Diseases, Obihiro University of Agriculture Veterinary Medicine, Inada-cho, Obihiro, Japan

[2]Department of Veterinary Medicine, Agriculture College of Yanbian University, Yanji, China

[3]College of Veterinary Medicine and Biomedical Sciences, Cavite State University, Indang, Philippines

[4]Department of Biochemistry and Molecular Biology, Faculty of Veterinary Medicine, Mansoura University, Egypt

[5]Central Laboratory, Institute of Tropical Medicine (NEKKEN), Nagasaki University, Nagasaki, Japan

[6]School of Basic Medicine, Hubei University of Arts and Science, Xiangyang, China

[7]Research Center for Asian Infectious Diseases, The University of Tokyo, Tokyo, Japan

***Correspondence:** Mingming Liu; Xuenan Xuan

Address: Longzhong Road No.296, Xiangyang, China; Nishi 11 Minami 39 Chome, Obihiro, Hokkaido

Telephone number: +8618904416800; +8109079036369

E-mail address: lmm_2010@hotmail.com; gen@obihiro.ac.jp

Competing interest: The authors have declared that no conflict of interest exists.

# These authors contributed equally to this work.

Abstract

Babesiosis is a disease brought on by intraerythrocytic parasites of the genus *Babesia*. Current chemotherapies are accompanied by side effects and parasite relapse. Therefore, it is crucial to develop highly effective drugs against *Babesia*. Cipargamin (CIP) has shown inhibition against apicomplexan parasites, mainly *Plasmodium* and *Toxoplasma*. This study evaluated the growth-inhibiting properties of CIP against *Babesia* spp. and investigated the mechanism of CIP on *B. gibsoni*. The half inhibitory concentration (IC_{50}) values of CIP against the *in vitro* growth of *B. bovis* and *B. gibsoni* were 20.2 ± 1.4 nM and 69.4 ± 2.2 nM, respectively. CIP significantly inhibited the growth of *B. microti* and *B. rodhaini in vivo.* Resistance was conferred by L921V and L921I mutations in BgATP4, which reduced the sensitivity to CIP by 6.1- and 12.8-fold. The inhibitory potency of CIP against BgATP4-associated ATPase activity was moderately reduced in mutant strains, with a 1.3-fold and 2.4-fold decrease in $BgATP4^{L921V}$ and $BgATP4^{L921I}$, respectively, compared to that of $BgATP4^{WT}$. An *in silico* investigation revealed reductions in affinity for CIP binding to $BgATP4^{L921V}$ and $BgATP4^{L921I}$ compared to $BgATP4^{WT}$. Resistant strains showed no significant cross-resistance to atovaquone (ATO) or tafenoquine succinate (TQ), with less than a onefold change in IC_{50} values. Combining CIP with TQ effectively eliminated *B. microti* infection in SCID mice with no relapse, and parasite DNA was not detected by qPCR within 90 days post-infection. Our findings reveal the efficacy of CIP as an anti-babesial agent, its limitations as a monotherapy due to resistance development, and the potential of combination therapy with TQ to overcome said resistance and achieve complete parasite clearance.

49 **Keywords:** Cipargamin; *Babesia* spp.; drug resistance; ATP4; mutation

50

Introduction

Babesia is an apicomplexan tick-transmitted hemoparasite, which not only impacts the livestock economy but also causes an emerging disease in humans (Jalovecka et al., 2019). *Babesia* is a global pathogen that is more prevalent in certain regions such as Asia, Europe, and North America. However, as climate change brings with it higher temperatures and humidity, ticks and their reservoir hosts are anticipated to expand northward for survival and activity (Gray and Ogden, 2021). The disease is known as babesiosis, commonly characterized by fever and hemolytic anemia, but chronic infections can be asymptomatic (Almazán et al., 2022). The fatality rate ranges from 1% among all cases to 3% among hospitalized cases, and as high as 20% in immunocompromised patients (Krause, 2019).

Currently, the most common drugs for the treatment of human babesiosis include a combination of atovaquone (ATO) plus azithromycin (AZI) or clindamycin (CLN) plus quinine (QUI) (Krause et al., 2021). Still, these recommended treatments often result in various problems. For instance, multiple mutations in the *B. microti* cytochrome b, which is targeted by ATO, were identified in patients with relapsing babesiosis (Holbrook et al., 2023; Krause et al., 2024; Lemieux et al., 2016; Marcos et al., 2022; Rogers et al., 2023; Rosenblatt et al., 2021; Simon et al., 2017). The combination of CLN and QUI is the last resort for patients with severe symptoms (Kletsova et al., 2017). Despite its efficacy, this combination can elicit adverse drug reactions (Vannier and Krause, 2012). The 8-aminoquinoline analog tafenoquine (TQ) was found to be effective in curing immunocompromised patients experiencing relapsing babesiosis caused by *B. microti* (Rogers et al., 2023). However, the efficacy of TQ treatment may vary between individuals and cases and its contraindication in patients with glucose-6-phosphate dehydrogenase (G6PD) deficiency limits its clinical use (Chu and Freedman, 2019). Due to the aforementioned issues, it is undoubtedly urgent to search for compounds that treat infections caused by *Babesia* spp. while simultaneously

76 minimizing the detrimental side effects of antibabesial drugs.

77 Spiroindolone cipargamin (CIP), a promising antimalarial, has been found to effectively
78 suppress the growth of all strains of *Plasmodium falciparum* and *P. vivax* with potency in the
79 low nanomolar ranges (Rosling et al., 2018; Rottmann et al., 2010). The assessment of the
80 drug indicated that CIP taken orally had good absorption, a long half-life, and exceptional
81 bioavailability (Schmitt et al., 2022). Following oral CIP treatment (30 mg daily for three
82 days) in adults with simple *P. falciparum* or *P. vivax* malaria, parasitemia was rapidly cleared
83 in a phase II trial (Schmitt et al., 2022). Currently, a clinical trial is being conducted for the
84 intravenous administration of CIP as a treatment for severe malaria patients (ClinicalTrials,
85 2024). CIP was also evaluated for treating toxoplasmosis as a second-line medicine in cases
86 where there are intolerable toxicity issues or allergies to the currently used treatments. Mice
87 infected with *Toxoplasma gondii* that were treated with CIP on the day of infection and the
88 following day had 90% fewer parasites five days post-infection (Zhou et al., 2014).

89 *Pf*ATP4, a P-type ATPase in *P. falciparum*, functions as a Na^+/H^+ transporter critical for
90 maintaining ionic balance (Spillman et al., 2013). Mutations in *Pf*ATP4 confer resistance to
91 CIP, which disrupts Na^+ homeostasis, leading to increased cytosolic Na^+ concentration and
92 various physiological changes, such as cytosolic alkalinization, osmotic swelling, etc.
93 (Mohring et al., 2022). These mutations reduce the Na^+-dysregulating effects of CIP and the
94 resting Na^+ levels. While *Pf*ATP4 is essential for *P. falciparum* survival, its homolog in *T.*
95 *gondii* (*Tg*ATP4) is less critical, as *T. gondii* experiences brief, high Na^+ exposure and can
96 survive without *Tg*ATP4 expression (Lehane et al., 2019).

97 Due to its excellent efficacy against other apicomplexan parasites, including *Plasmodium*
98 spp., and its ability to target parasite ATP4—a conserved protein essential for ion homeostasis
99 in apicomplexan organisms—we hypothesize that CIP could also effectively inhibit *Babesia*
100 spp., a related apicomplexan parasite. Therefore, the objectives of this study were to

101 determine whether CIP could inhibit the growth of *Babesia* spp., namely *B. bovis* and *B.*
102 *gibsoni in vitro* and *B. microti* and *B. rodhaini in vivo*, and identify the inhibitory mechanisms
103 of CIP on *Babesia* parasites.
104

105 **Results**

106 **Inhibitory efficacy of CIP on *B. bovis* and *B. gibsoni in vitro***

107 *In vitro* efficacy of CIP against *B. bovis* and *B. gibsoni* showed a steep growth inhibition
108 curve with half inhibitory concentration (IC_{50}) values of 20.2 ± 1.4 nM (Figure 1A) and 69.4
109 ± 2.2 nM (Figure 1B), respectively. The 50% cytotoxic concentration (CC_{50}) value of CIP on
110 Madin-Darby canine kidney (MDCK) cells and human foreskin fibroblasts (HFF) were 38.7
111 ± 2.0 μM and 70.8 ± 4.9 μM (Figure supplement 1), respectively. Based on these values, the
112 predicted selectivity indices (SIs), which reflect the drug's safety and specificity, were
113 calculated to be greater than 500. Furthermore, at a concentration of 100 μM, CIP exhibited a
114 low erythrocyte hemolysis rate of 0.11 ± 0.03 % (data not shown).

115 **CIP effect on *B. microti* and *B. rodhaini* infections *in vivo***

116 Concurrently, CIP showed effective inhibition on *B. microti* and *B. rodhaini in vivo*. The
117 parasitemia of *B. microti*-infected BALB/c mice increased dramatically in the vehicle-treated
118 control group and peaked at 10 days postinfection (DPI) (38.55 ± 4.32%) (Figure 1C). On the
119 other hand, seven days of treatment with CIP (20 mg/kg) or atovaquone (ATO) plus
120 azithromycin (AZI) administered orally resulted in a significantly lower peak parasitemia,
121 1.06 ± 0.20% and 1.61 ± 0.20%, respectively (Figure 1C). Hematocrit (HCT) variations were
122 tracked every 4 days as an indicator of anemia in *B. microti*-infected mice. The
123 vehicle-treated group showed a drop in HCT levels at 12 DPI and 16 DPI ($P < 0.01$) (Figure
124 1D). No significant reduction in HCT levels was observed in the CIP-treated group or the
125 ATO plus AZI-treated group (Figure 1D). This indicates that the administration of CIP could

126 control *B. microti* infection and prevent anemia from developing in *B. microti*-infected mice.
127 BALB/c mice infected with *B. rodhaini* treated with sesame oil or ATO plus AZI showed high
128 parasitemia, 90.73 ± 1.97%, and 86.23 ± 3.06%, respectively (Figure 1E), and all mice died
129 within 7 DPI (Figure 1F). CIP treatment in *B. rodhaini*-infected mice precluded the
130 emergence of parasitemia for the following eight days (Figure 1E), which led to 66.67% of
131 mice surviving the challenge infection (Figure 1F). At 12 DPI, parasites had recurred in all
132 CIP-treated *B. rodhaini*-infected mice (10.32 ± 15.51%), which were eventually cleared as
133 indicated by undetectable parasites at 18 DPI (Figure 1E).

134 **Identification of *B. gibsoni* ATP4 mutation in CIP-resistant strains**

135 After being exposed to CIP at increasing concentrations up to 10 times the IC_{50}, the resistant
136 parasites in two of the culture wells were able to regrow. We sequenced the *B. gibsoni* ATP4
137 gene from the wild-type and two resistant strains. The wild-type strain has a C at nucleotide
138 2,761, which translates to leucine (Figure 2A). In one resistant strain, a single nucleotide
139 variant (SNV) in BgATP4 with a substitution at position 2,761 (from C to G) was found − a
140 nonsynonymous coding change from leucine to valine (L921V) (Figure 2B). In another
141 resistant strain, the mutation occurred in the same position. However, the nucleotide
142 substitution was from C to A, and the coding changed from leucine to isoleucine (L921I)
143 (Figure 2C). Next-generation sequencing (NGS) revealed that for $Bgatp4^{2761C>G}$, 99.97% of
144 7,960 reads were G at nucleotide 2,761, and for $Bgatp4^{2761C>A}$, 99.92% of 7,862 reads were A
145 at nucleotide 2,761 (Figure 2D). $BgATP4^{L921V}$ and $BgATP4^{L921I}$ lines were tested for their
146 susceptibility to CIP, and had IC_{50} values of 421.0 ± 15.9 nM and 887.9 ± 62.0 nM,
147 respectively (Figure 2E). These findings demonstrate a 6.1- and 12.8-fold reduction in CIP
148 sensitivity of the resistant parasite lines $BgATP4^{L921V}$ and $BgATP4^{L921I}$.

149 **The effect of CIP on $BgATP4^{WT}$, $BgATP4^{L921V}$ and $BgATP4^{L921I}$ function**

150 Microscopic observation of thin blood smears was performed to determine the morphological

151 changes of *B. gibsoni* exposed to CIP. The CIP-treated parasites became swollen after
152 incubation with the drug for 72 h (Figure 3A). For both the treatment and control groups, one
153 hundred parasites were measured. The mean size of treated parasites was notably bigger than
154 the parasites in the untreated group ($P < 0.0001$) (Figure 3B). Significant vacuolization was
155 observed in the cytoplasm of parasites in the CIP-treated group, as revealed by transmission
156 electron microscopy (TEM). Despite this, the nuclear membrane structure and parasitic
157 membranes remained intact until the parasites were completely destroyed (Figure 3C). The
158 addition of the ATP4 inhibitor CIP resulted in a time-dependent increase in the concentrations
159 of $[Na^+]_i$ in wild-type *B. gibsoni*, with improved signal-to-noise ratios at the higher drug
160 concentration of 20 nM (Figure 3D). We observed that the Na^+ concentrations in both
161 $BgATP4^{L921V}$ and $BgATP4^{L921I}$ lines were lower when compared with those of the control
162 $BgATP4^{WT}$ line after being exposed to 20 nM CIP for 20 min, with a significantly lower Na^+
163 concentration in $BgATP4^{L921I}$ ($P = 0.0087$) (Figure 3F). We also demonstrated here that the
164 addition of CIP in wild-type *B. gibsoni* caused an increase in the cytosolic pH (Figure 3E).
165 Specifically, 4 min after the drug was added, the average pH of the 20 nM CIP group reached
166 as high as 7.278, while the 1 nM CIP group reached 7.089 and the untreated group reached
167 7.062 (Figure 3E). The pH values of the 20 nM CIP group were consistently higher than those
168 of the other two groups, although declining with time (Figure 3E). In resistant lines, a 20-min
169 exposure to 20 nM CIP caused small changes in the pH values compared to the wild-type line,
170 with the $BgATP4^{L921I}$ line (7.048 ± 0.042) having a notably lower pH value ($P = 0.0229$)
171 (Figure 3G).

172 **Sensitivity of BgATP4-associated ATPase activity to CIP in $BgATP4^{WT}$, $BgATP4^{L921V}$,**
173 **and $BgATP4^{L921I}$**

174 The BgATP4-associated ATPase activity in erythrocytes infected with $BgATP4^{WT}$ (6.31 ±
175 1.20 nmol Pi/mg protein/min), measured in the presence of 150 mM Na^+, was higher than

176 those observed in BgATP4^{L921V} (5.11 ± 0.50 nmol Pi/mg protein/min) and BgATP4^{L921I} (4.58
177 ± 0.53 nmol Pi/mg protein/min) (P = 0.04) (Figure 3H).
178 We further investigated the concentration-dependent inhibition of BgATP4-associated ATPase
179 activity by CIP in wild-type and mutant parasites. In membranes prepared from *B.gibsoni*,
180 CIP inhibited BgATP4-associated ATPase activity with IC_{50} values of 111.4 ± 31.8 nM for
181 BgATP4^{WT}, 149.8 ± 21.7 nM for BgATP4^{L921V}, and 269.5 ± 29.8 nM for BgATP4^{L921I}. The
182 potency of CIP in inhibiting BgATP4-associated ATPase activity was reduced by 1.3-fold and
183 2.4-fold in membranes prepared from BgATP4^{L921V} and BgATP4^{L921I}, respectively, compared
184 to BgATP4^{WT} (Figure 3I).

185 **Multiple sequence alignment of *Babesia* ATP4 and molecular docking**

186 The whole amino acid sequence of *B. gibsoni* ATP4 (GenBank: KAK1443404.1) shared
187 identity values of 29.75%, 49.40%, 49.67%, 62.21%, and 52.47% with *Homo sapiens* ATP4
188 (GenBank: NM_000704.3), *P. falciparum* ATP4 (GenBank: PF3D7_1211900), *T. gondii*
189 ATP4 (GenBank: XP_018635122.1), *B. bovis* ATP4 (PiroplasmaDB: BBOV_IV010020), and
190 *B. microti* ATP4 (GenBank: BMR1_03g01005), respectively (Figure supplement 2).
191 The pLDDT (predicted Local Distance Difference Test) value of BgATP4^{WT} prediction was
192 80.7 using Colab-fold. Multiple potential binding sites for CIP were revealed by blind
193 docking throughout the whole protein surface (Figure supplement 3). CIP binds in close
194 proximity to L921, as demonstrated by focused docking on this area (Figure 4A). The
195 contribution of each residue to the predicted binding affinity in either mutant structure was
196 reduced; the precise values of BgATP4^{WT} (Figure 4B), BgATP4^{L921V} (Figure 4C), and
197 BgATP4^{L921I} (Figure 4D) were -6.43, -6.40 and -6.26 kcal/mol, respectively. The interactions
198 of CIP from each docking simulation are shown in Table supplement 3.

199 **Cross-resistance of BgATP4^{L921V} and BgATP4^{L921I} mutants to ATO and TQ**

200 The BgATP4^{WT}, BgATP4^{L921V}, and BgATP4^{L921I} lines were tested for their susceptibility to

201 ATO and TQ. The IC_{50} values for these lines were 380.1 ± 3.1 nM, 412.9 ± 5.4 nM, and 360.3
202 ± 7.9 nM, respectively, for ATO (Figure 5A), and 39.5 ± 0.4 μM, 29.9 ± 1.4 μM, and 39.3 ±
203 0.3 μM, respectively, for TQ (Figure 5B). The IC_{50} values for both ATO and TQ in the
204 resistant strains showed only slight changes compared to the wild-type strain, with less than a
205 onefold difference. This minimal variation suggests that the resistant strain has a mild
206 alteration in susceptibility to ATO and TQ, but not enough to indicate strong resistance or
207 significant cross-resistance.

208 **Combination treatment of CIP plus TQ in SCID mice with *B. microti* infection**

209 The parasitemia of *B. microti*-infected SCID mice in the vehicle group increased dramatically,
210 peaking at 10 DPI (77.03 ± 2.45%) (Figure 5C). Although the trend showed a subsequent
211 decline, the parasitemia remained around 50% until the mice were euthanized at 90 DPI.
212 Treatment with CIP (20 mg/kg) initially reduced parasitemia to undetectable by 18 DPI.
213 However, a relapse occurred, with parasitemia increasing rapidly and stabilizing at levels
214 comparable to the vehicle group during the subsequent observation period. Notably, no
215 mutations were detected in the relapsed *B. microti* parasites from SCID mice (data not
216 shown). In contrast, parasitemia was completely cleared in the TQ and CIP plus TQ groups
217 by 8 DPI and 6 DPI, respectively, with no parasites observed under the microscope thereafter.
218 qPCR analysis at 90 DPI detected parasite DNA in all groups except the CIP plus TQ group
219 (Figure 5D).

220 **Discussion**

221 The repositioning of antimalarial drugs is critical in developing novel strategies for treating
222 babesiosis. CIP is a novel compound that inhibits *Plasmodium* development by targeting
223 ATP4 and has been extensively tested in Phase 1 and Phase 2 clinical trials (Qiu et al., 2022).
224 Since ATP4 is conserved across apicomplexans, including *Babesia* species, our study aimed
225 to repurpose the antimalarial CIP by assessing its efficacy on *Babesia* species (Lehane et al.,

226 2019). The IC_{50} values of CIP against *B. bovis* and *B. gibsoni in vitro* were lower than the
227 previously reported IC_{50} value of TQ (Carvalho et al., 2020; Ji et al., 2022b) and ATO against
228 *B. gibsoni* (Matsuu et al., 2004). The present investigation also demonstrated that the
229 inhibitory effects of CIP on *B. microti*-infected BALB/c mice were comparable to that of
230 ATO plus AZI, the combination recommended by the CDC in the United States. CIP was also
231 proven to protect mice from the deadly *B. rodhaini* infection, with a survival rate of up to
232 67%, as recorded in the current trial. These results suggest that CIP may be a potential
233 chemotherapy candidate for babesiosis.

234 In a previous study, the *P. falciparum* Dd2 strain that acquired resistance to CIP carried the
235 G358S mutation in the *Pf*ATP4 protein, a *P. falciparum* P-type Na^+ ATPase (Qiu et al., 2022).
236 The vital protein ATP4 is found in the parasite plasma membrane and is specific to the
237 subclass of apicomplexan parasites (Mohring et al., 2022). To date, *in vitro* evolution
238 experiments using CIP have produced at least 18 parasite lines with various *Pf*ATP4
239 mutations (Lee and Fidock, 2016; Rottmann et al., 2010). In another study involving *T.*
240 *gondii*, a cell line that carried the mutation G419S in the *Tg*ATP4 gene was 34 times less
241 susceptible to CIP than that of *Tg*ATP4^{WT} (Qiu et al., 2022). It follows that there is a
242 significant possibility that resistant *Babesia* parasites will emerge from CIP exposure. In this
243 study, we successfully produced two CIP-resistant strains using six independent selections.
244 The newly discovered L921V and L921I mutations in BgATP4 decreased the CIP sensitivity
245 by 6.1 and 12.8 times, respectively. We provided compelling evidence that natural variety
246 mutations L921V and L921I in BgATP4 significantly affected the protein's susceptibility to
247 CIP inhibition, albeit the mutational sites were different from those of *P. falciparum* and *T.*
248 *gondii*. Based on our observation, the growth and generation rates of the mutant strains are
249 comparable to those of the wild-type strain.

250 Although ATP4 was initially recognized as a Ca^{2+} transporter (Krishna et al., 2001), current

251 evidence suggests that ATP4 functions as an ATPase for exporting Na^+ while importing H^+
252 (Mohring et al., 2022), as well as causing a variety of other physiological perturbations
253 including an increase in the volume of parasites and infected erythrocytes due to the osmotic
254 impact of the $[Na^+]_{cyt}$ increase (Dennis et al., 2018), a decline in cholesterol extrusion from
255 the parasite plasma membrane as a result of the increase in $[Na^+]_{cyt}$ (Das et al., 2016), and an
256 intensified rigidity of erythrocytes infected with ring-stage parasites (Zhang et al., 2016). In
257 this study, the CIP-exposed wild-type *B. gibsoni* became swollen, which was identical to a
258 prior study on *P. falciparum* (Dennis et al., 2018). Interestingly, transmission electron
259 microscopy (TEM) analysis of parasites incubated with CIP revealed ultrastructural
260 alterations characterized by significant vacuole formation in the cytoplasm, a hallmark of
261 stress or early stages of cell death. These changes were similar to those observed in *B. bovis*
262 treated with clotrimazole and ketoconazole, which ultimately led to growth inhibition or
263 parasite death (Bork et al., 2003). Despite the vacuolization, the structural integrity of the
264 nucleus and membranes was maintained, suggesting a gradual process where vacuolization
265 precedes complete destruction of the parasite. One explanation is the swelling of the isolated
266 parasites, which can be ascribed to the osmotic consequences of Na^+ uptake and is contingent
267 upon the presence of Na^+ in the external environment.

268 The output of Na^+ and input of H^+ diminished upon CIP-induced inhibition of *Pf*ATP4, and
269 the continued outflow of H^+ via V-type H^+-ATPase led to an alkalinization that ultimately
270 killed the parasites (Spillman et al., 2013). Our capacity to measure a time-dependent
271 increase in the concentration of $[Na^+]_i$ and pH value for wild-type *B. gibsoni* facilitated us to
272 gain insight into the basic mechanisms of CIP on $BgATP4^{WT}$ function. Furthermore, our
273 results corroborate internal alkalinization as the main factor in *Babesia* death and support our
274 hypothesis that the swollen isolated parasites were produced by Na^+ absorption. To explore
275 further how mutations in BgATP4 are associated with the upregulation of the parasite's $[Na^+]_i$

276 and $[H^+]_i$, we tested two BgATP4-mutant lines that were chosen previously with BgATP4
277 inhibitors ($BgATP4^{L921V}$ and $BgATP4^{L921I}$). Due to the presence of L921V and L921I
278 mutations in drug-resistant strains of BgATP4, the concentration of Na^+ did not increase as
279 much as it would have in the wild-type strain following the addition of 20 nM CIP for 20 min.
280 As intraerythrocytic alkalinization rises, the same outcome happens. From these results, we
281 deduced how natural mutations in BgATP4 may affect ATP4 inhibitor susceptibility by
282 dysregulating H^+ and Na^+ balance, which helped parasites survive in a relatively high
283 concentration of CIP. An illustration of the putative processes for regulating Na^+ and H^+ in
284 erythrocytes infected with the *Babesia* parasite is presented in Figure supplement 4.

285 In a previous study's isolated membrane assay, CIP was found to be more effective at
286 inhibiting parasite development than *Pf*ATP4-associated ATPase activity and reduced
287 sensitivity of *Pf*ATP4-associated ATPase activity to the medication was associated with a
288 decrease in parasite susceptibility to CIP (Rosling et al., 2018). In our study, the higher
289 resistance to CIP-mediated inhibition of parasite proliferation observed in $BgATP4^{L921I}$
290 compared to $BgATP4^{L921V}$ correlated with a higher resistance of BgATP4-associated ATPase
291 activity to the drug. These findings provide additional evidence that the ATPase activity
292 measured in this study corresponds to the activity of the BgATP4 protein.

293 According to studies using the *Pf*ATP4 model for molecular docking, the G358S mutation
294 results in a steric clash that lowers CIP's binding affinity (Qiu et al., 2022). The results from
295 the current study were similar to the *Pf*ATP4 model. The molecular docking was constructed
296 using a ColabFold model of wild-type BgATP4, which predicted the binding mode and
297 affinity between ATP4 protein and the ligand to provide a possible mechanistic explanation. It
298 suggested that the L921V mutation caused changes at the atomic level, whereas the L921I
299 mutation created a steric clash that reduced the binding affinity of CIP. The predicted affinity
300 score of the L921I mutation was lower than that of the L921V mutation. Thus, it is possible

301 that CIP had a weaker binding to BgATP4^{L921I} than to BgATP4^{L921V}. These findings are
302 consistent with the results obtained from measuring the IC_{50} of the drug against parasites with
303 the L921V and L921I mutations.

304 While CIP shows promise as an antibabesial agent, the emergence of resistance emphasizes
305 the importance of rational drug use and the development of combination therapies. Our
306 results demonstrate that CIP did not exhibit cross-resistance with ATO or TQ, as IC_{50} values
307 for ATO and TQ in resistant strains showed minimal changes (<1-fold) compared to the
308 wild-type strain. This observation suggests that CIP could be effectively combined with other
309 antibabesial drugs to reduce the risk of resistance development. Previous studies have also
310 reported that a single dose of TQ may not be sufficient to prevent parasite relapse in
311 immunocompromised hosts, recommending either repeated TQ administration or
312 combination therapy with other antibabesial agents to address this issue (Mordue et al., 2019).
313 Supporting this approach, our study demonstrates that the combination of CIP plus TQ
314 effectively cleared *B. microti* infections in SCID mice, with no detectable parasitemia or
315 DNA observed at 90 DPI, indicating complete parasite elimination.

316 This preclinical finding underscores the potential of the CIP plus TQ combination as a
317 viable treatment strategy for babesiosis, especially in cases where monotherapy is ineffective.
318 Further studies are needed to fully explore the pharmacokinetics, long-term efficacy, and
319 potential side effects of such combinations in clinical settings, ultimately facilitating
320 optimized therapeutic strategies.

321 In summary, our findings provide a comprehensive understanding of CIP's efficacy,
322 mechanism of resistance, and identifying strategies to enhance its therapeutic potential. The
323 combination of CIP with drugs like TQ offers a promising approach to combat babesiosis and
324 mitigate the development of resistance.

325

326 **Materials and methods**

327 **Parasite culture**

328 The parasites *B. gibsoni* Oita strain and *B. bovis* Texas strain were *in vitro* cultured in 24-well
329 plates and maintained in an atmosphere of 5% CO_2 and 5% O_2 at 37 °C (Liu et al., 2018). For
330 the *in vivo* studies, *B. microti* Peabody mjr strain-(ATCC PRA-99™) and *B. rodhaini*
331 Australia strain-infected RBCs (iRBCs), which were collected and diluted with
332 phosphate-buffered saline (PBS) when the parasitemia levels in the donor mice reached
333 ~20% and 50%, respectively, and were intraperitoneally injected into BALB/c mice. Each
334 BALB/c mouse was infected with 1.0×10^7 *B. microti* or *B. rodhaini* iRBCs for the *in vivo*
335 trials (Ji et al., 2022a).

336 ***In vitro* cytotoxicity of CIP and hemolysis rate in canine erythrocytes**

337 Cultures of Madin-Darby canine kidney (MDCK) cells and human foreskin fibroblasts (HFF)
338 were maintained at 37 °C under an atmosphere of 5% CO_2 and 5% O_2 and the cytotoxic effect
339 of CIP (MedChem Express, Tokyo, Japan) was assessed using a cell viability assay by CCK-8
340 (Dojindo, Japan) as described previously (Li et al., 2023). The selectivity index is calculated
341 as the ratio between the half maximal inhibitory concentration (IC_{50}) and the 50% cytotoxic
342 concentration (CC_{50}) values.

343 Canine erythrocytes were collected from healthy beagle dogs raised in NRCPD and stocked
344 in Vega y Martinez (VYM) phosphate-buffered saline solution at 4 °C (Vega et al., 1985). A
345 canine erythrocyte hemolysis assay was performed at concentrations of 0.1, 1, 5, 10, 25, 50,
346 and 100 μM as previously described (Ariefta et al., 2022).

347 **Evaluation of the efficacy of CIP against *Babesia* parasites *in vitro***

348 The efficacy of CIP against *B. gibsoni* and *B. bovis* was determined using a fluorescence
349 assay, as previously described (Guswanto et al., 2014). The IC_{50} values were determined from
350 the fluorescence values and by non-linear regression analysis (curve fit) in GraphPad Prism 9

351 (GraphPad Software Inc., USA).

352 **Chemotherapeutic effects of CIP against *Babesia* infections *in vivo***

353 CIP was evaluated on *B. microti*- and *B. rodhaini*-infected mice, as previously described
354 (Ndayisaba et al., 2021; Tuvshintulga et al., 2022). When *B. microti*- and *B. rodhaini*-infected
355 mice had a 1% average parasitemia at 4 and 2 days postinfection (DPI), respectively, the drug
356 treatments were administered and continued for seven days. Three groups of *B.*
357 *microti*-infected mice were administered different treatments. The CIP group (n = 6) and the
358 ATO plus AZI group (n = 6) were orally treated with 20 mg/kg CIP and 20 mg/kg ATO plus
359 20 mg/kg AZI (Sigma, Tokyo, Japan), respectively. All drugs were prepared in sesame oil.
360 The infected mice of the vehicle group (n = 6) orally received 0.2 mL of sesame oil as the
361 control. Eighteen mice infected with *B. rodhaini* were likewise placed into three groups for
362 treatment, and they received the same treatments as the mice infected with *B. microti*. A light
363 microscope (Nikon, Japan) and a hematology analyzer (Celltac α MEK-6450, Nihon Kohden
364 Corporation, Tokyo, Japan) were used to assess the parasitemia and hematocrit levels every
365 two and four days, respectively.

366 **Selection of CIP-resistant *B. gibsoni in vitro***

367 Selections were initiated by exposing six independent flasks, each containing 10 μL (5×10^6)
368 *B. gibsoni* iRBCs mixed with 40 μL (4×10^8) RBCs into a 450 μL culture medium, which
369 contained increasing concentrations of CIP: 5, 10, 20, 30 to 694 nM ($10\times IC_{50}$). The medium
370 containing CIP was replaced daily until parasites treated with $10\times IC_{50}$ CIP reached
371 multiplication rates that were approximately comparable to those of the untreated controls
372 (Hwang et al., 2010). Then, to evaluate the decreased sensitivity to CIP, IC_{50} values of
373 resistant strains were determined by nonlinear regression using the GraphPad Prism software.

374 **Detection of *B. gibsoni* ATP4 gene mutations**

375 The genomic DNA of the mutant parasites was extracted and sequenced (Ji et al., 2022a). The

376 primer sets used for sequencing are listed in Table supplement 1. The single nucleotide
377 variants were identified by pairwise alignment to the BgATP4^{WT} sequence (GenBank:
378 JAVEPI010000002.1). Next-generation sequencing (NGS) was performed to detect the ratio
379 of wild-type to mutant parasites by using the Illumina NovaSeq6000 sequencing platform
380 (Jeon et al., 2021).

381 **Morphological changes in CIP-treated *in vitro* cultured *B. gibsoni***

382 A microscopy assay was used to detect the morphological changes of wild-type *B. gibsoni*
383 after exposure to 50 nM CIP for three consecutive days (Liu et al., 2021; Tayebwa et al.,
384 2018). At 4 days post-treatment, ImageJ software was used to measure the sizes of 100
385 randomly selected parasites in the CIP-treated group and the control group on Giemsa-stained
386 blood smears. After treating the parasites as described above, iRBCs were fixed in GA
387 fixation buffer (2% glutaraldehyde in 0.1 M sodium cacodylate buffer containing 1 mM
388 $CaCl_2$ and 1 mM $MgCl_2$), then stored in rinse buffer (0.1 M sodium cacodylate buffer
389 containing 1 mM $CaCl_2$ and 1 mM $MgCl_2$) at 4 ºC for transmission electron microscopy
390 (TEM) analysis (Hidayati et al., 2023).

391 **Parasites $[Na^+]_i$ and pH_i measurements**

392 For both $[Na^+]_i$ and pH_i measurements, the wild-type and mutant parasites were initially
393 separated from erythrocytes by treatment with saponin (0.05% [wt/vol]) for 5 min (Saliba and
394 Kirk, 1999). The Na^+-sensitive fluorescent dye SBFI (Thermo Fisher Scientific; product
395 S1263) was used to quantify intracellular sodium ($[Na^+]_i$). Saponin-isolated parasites (at
396 1×10^8 parasites/mL) were loaded with SBFI (5 μM; in the presence of 0.02% w/v Pluronic
397 F127) for 1 hr at room temperature (RT) (Spillman et al., 2013). Thereafter, SBFI-loaded
398 parasites were resuspended in physiological saline (120 mM NaCl, 5 mM KCl, 25 mM
399 HEPES, 20 mM D-glucose, and 1 mM $MgCl_2$ [pH 7.1]) at RT in the presence or absence of
400 CIP. A 96-well microtiter plate was filled with around 200 μL of parasite suspension per well.

401 The dye-loaded cells fluoresced at 515 nm after being stimulated at 340 and 380 nm.
402 Parasites loaded with SBFI were suspended in calibration buffers containing [Na^+] values
403 ranging from 0 to 140 mM (pH 7.1) to establish calibration curves (Diarra et al., 2001).
404 The cytosolic pH of wild-type and mutant strains was measured using the pH-sensitive
405 fluorescent dye BCECF [2',7'-bis-(2-carboxyethyl)-5-(and-6)- carboxyfluorescein] (Biotium;
406 product 51011). The BCECF was added to saponin-isolated parasites by suspension (1×10^8
407 parasites/mL) and incubated for 20 minutes at 37 °C in RPMI-1640 culture medium (Gibco,
408 USA) (Saliba and Kirk, 1999). Thereafter, the parasites loaded with dye were rinsed thrice
409 (12,000 × g, 1 min) in RPMI-1640 culture medium, then resuspended in physiological saline
410 (as previously mentioned) with or without various concentrations of CIP. A 96-well microtiter
411 plate was filled with around 200 µL of parasite suspension per well. The dye-loaded cells
412 fluoresced at 520 nm after being stimulated at 440 and 490 nm. A pH calibration was carried
413 out for each experiment (Mohring et al., 2022).

414 **Measurements of membrane ATPase activity**

415 Membranes from isolated *B. gibsoni* were prepared by lysing the parasites in ice-cold
416 deionized water containing 7 × Protease Inhibitor Cocktail Tablets (Roche, Germany). The
417 membrane preparation was then washed three times with ice-cold deionized water, with
418 protease inhibitors included in the first two washes (Qiu et al., 2022). Protein concentrations
419 in the membrane samples were determined using a Bradford assay. The production of
420 inorganic phosphate (Pi) from ATP hydrolysis was measured using the Malachite Green
421 Phosphate Assay (BioAssay Systems, USA). Membrane preparations were diluted in either a
422 high Na^+ solution (final reaction conditions: 150 mM NaCl, 20 mM KCl, 2 mM $MgCl_2$, 50
423 mM Tris, pH 7.2) or a Na^+-free solution (final reaction conditions: 150 mM choline chloride,
424 20 mM KCl, 2 mM $MgCl_2$, 50 mM Tris, pH 7.2) to achieve a final protein concentration of
425 40 µg/mL. CIP was added at the concentrations specified in the respective figure legends.

426 Reactions were conducted according to the manufacturer's protocol provided with the assay
427 kit.

428 **Multiple ATP4 sequence alignment and molecular docking**

429 *B. gibsoni* ATP4 (GenBank: KAK1443404.1), *B. bovis* ATP4 (PiroplasmaDB:
430 BBOV_IV010020), *B. microti* ATP4 (GenBank: BMR1_03g01005), *T. gondii* ATP4
431 (GenBank: XP_018635122.1), and *Homo sapiens* ATP4 (GenBank: NM_000704.3)
432 sequences were obtained by a homology search using *P. falciparum* ATP4 (GenBank:
433 PF3D7_1211900). Sequence alignment was analyzed using MUSCLE in Jalview v2.11.3.2
434 software and BLAST (http://www.ncbi.nlm.nih.gov/BLAST/).

435 AlphaFold was used to predict the structure of $BgATP4^{WT}$ (Jumper et al., 2021). Using the
436 GROMACS 2021 Molecular Dynamics package, the energy minimization was carried out
437 following the model's generation (Lindahl et al., 2021). The mutations were produced by
438 using Charmm-GUI PDB reader (Jo et al., 2014). PyMOL (version 2.0 Schrödinger, LLC)
439 was used to confirm the position of the mutation site (center: -20.367, 10.904, 9.435; size:
440 30×30×30) (Trott and Olson, 2010). The ligand molecules CIP was downloaded from
441 PubChem (CID 44469321 (https://pubchem.ncbi.nlm.nih.gov/compound/44469321). The
442 ligand was used to dock with Gnina (Eberhardt et al., 2021). The affinity score and binding
443 pose were chosen only from the highest CNN (convolutional neural network) score results
444 from docking simulations. The models were visualized using the PyMOL Molecular Graphic
445 System and Discovery Studio.

446 **Cross-resistance to TQ and ATO in mutant parasites**

447 The efficacy of TQ and ATO against $BgATP4^{WT}$, $BgATP4^{L921V}$, and $BgATP4^{L921I}$ was
448 evaluated using a fluorescence assay, as described above. The IC_{50} values were calculated
449 from the fluorescence values using non-linear regression analysis (curve fitting) in GraphPad
450 Prism 9 (GraphPad Software Inc., USA).

451 **Efficacy of CIP plus TQ combination therapy in SCID mice infected with *B. microti***

452 Twenty 6-week-old female immunocompromised mice (C.B-17/IcrJcl-Prkdcscid strain,
453 CLEA Japan, Inc.) were intraperitoneally injected with 1.0×10^7 of *B. microti*-infected blood
454 cells (Tuvshintulga et al., 2022). When the average parasitemia across all mice reached 1%
455 (at 4 DPI), the drug treatments were initiated. The CIP group (n = 5) was orally administered
456 20 mg/kg CIP for seven days. The TQ group (n = 5) was orally administered a single dose of
457 20 mg/kg TQ. The CIP plus TQ group (n = 5) received the combination treatment, following
458 the dosage and administration methods described above. The vehicle group (n = 5) orally
459 received 0.2 mL of sesame oil as the control. Thin blood smears were prepared every other
460 day and examined under a light microscope to determine parasitemia levels.

461 **qPCR analysis**

462 To further verify the presence or absence of *B. microti* DNA in treated SCID mice, real-time
463 quantitative PCR analysis was performed as described previously (Vydyam et al., 2024).
464 Briefly, genomic DNA was extracted from blood samples (200 μl) collected at 90 DPI and
465 subjected to qPCR analysis using SYBR Green I, targeting a highly conserved region of
466 *Babesia* mitochondrial genome (mtDNA). Primers used were: Bmic-F
467 5′-TTGCGATAGTAATAGATTTACTGC-3′ and B-lsu-R2
468 5′-TCTTAACCCAACTCACGTACCA-3′ (Qurollo et al., 2017). The reaction mixture
469 consisted of: 1 × Advanced Universal SYBR Green Super Mix (2 ×) (1725270; Bio-Rad); 0.5
470 μM of each primer, and 100 ng of genomic DNA.

471 **Detection of *B. microti* ATP4 gene mutations in relapsed infected SCID mice**

472 The genomic DNA of the mutant parasites was extracted and sequenced (Ji et al., 2022a). The
473 primer sets used for sequencing are listed in Table supplement 2. The single nucleotide
474 variants were confirmed by pairwise alignment to the *Bm*ATP4^{WT} sequence (GenBank:
475 BMR1_03g01005).

Statistical analysis

Data analysis, namely one-way analysis of variance (ANOVA) and two-tailed unpaired t-tests, was performed using GraphPad Prism (La Jolla, CA, USA) version 9. A P value of <0.05 was considered a statistically significant result.

Acknowledgments

This work was supported by a Grant-in-Aid for Scientific Research (22H0250906), the JSPS Core-to-Core program, both from the Ministry of Education, Culture, Sports, Science, and Technology of Japan, and a grant from the Strategic International Collaborative Research Project (JPJ008837) promoted by the Ministry of Agriculture, Forestry, and Fisheries of Japan, and International Science and Technology Cooperation Project of Hubei Province (2024EHA018).

Declaration of competing interest

The authors declare that they have no known competing financial interests or personal relationships that could have appeared to influence the work reported in this paper.

Author contributions

Hang Li, Investigation, Data curation, Formal analysis, Writing – original draft, Writing – review & editing; Shengwei Ji, Methodology, Investigation, Software, Validation; Nanang R. Ariefta, Methodology, Software, Formal analysis; Eloiza May S. Galon, Visualization, Writing – review & editing; Shimaa AES El-Sayed, Methodology, Visualization; Thom Do, Methodology, Investigation; Lijun Jia, Data curation, Visualization; Miako Sakaguchi, Methodology, Visualization; Masahito Asada, Investigation, Visualization; Yoshifumi

Nishikawa, Methodology, Resources; Xin Qin, Methodology, Data curation; Mingming Liu, Conceptualization, Methodology, Investigation, Resources, Data curation, Funding acquisition, Supervision, Writing – review & editing; Xuenan Xuan, Conceptualization, Methodology, Validation, Formal analysis, Supervision, Project administration, Writing – review & editing.

Ethics

All animal experiments were performed according to the Guide for the Care and Use of Laboratory Animals of Obihiro University of Agriculture and Veterinary Medicine, which was also approved by the Committee on the Ethics of Animal Experiments at the Obihiro University of Agriculture and Veterinary Medicine, Japan (permit numbers: animal experiment, 22-145 and 23-132; DNA experiment, 2207 and 2208; pathogen, 202308 and 202306).

References

Almazán C, Scimeca RC, Reichard MV, Mosqueda J. 2022. Babesiosis and Theileriosis in North America. *Pathogens* **11**:168. doi:10.3390/pathogens11020168

Ariefta NR, Pagmadulam B, Nihei C, Nishikawa Y. 2022. Sparsomycin exhibits potent antiplasmodial activity *in vitro* and *in vivo*. *Pharmaceutics* **14**:544. doi:10.3390/pharmaceutics14030544

Bork S, Yokoyama N, Matsuo T, Claveria FG, Fujisaki K, Igarashi I. 2003. Clotrimazole, ketoconazole, and clodinafop-propargyl inhibit the *in vitro* growth of *Babesia bigemina* and *Babesia bovis* (Phylum Apicomplexa). *Parasitology* **127**:311–315. doi:10.1017/S0031182003003895

Carvalho LJM, Tuvshintulga B, Nugraha AB, Sivakumar T, Yokoyama N. 2020. Activities of artesunate-based combinations and tafenoquine against *Babesia bovis in vitro* and *Babesia microti in vivo*. *Parasites Vectors* **13**:362. doi:10.1186/s13071-020-04235-7

Chu CS, Freedman DO. 2019. Tafenoquine and G6PD: a primer for clinicians. *J Travel Med* **26**:taz023. doi:10.1093/jtm/taz023

ClinicalTrials.gov [Internet]. Bethesda (MD): National Library of Medicine (US). Identifier

NCT04675931, To evaluate efficacy, safety, tolerability and PK of intravenous cipargamin in participants with severe *Plasmodium falciparum* malaria; 2024 Feb 29 [cited 2024 Apr 9]. Available from: https://clinicaltrials.gov/study/NCT04675931

Das S, Bhatanagar S, Morrisey JM, Daly TM, Burns JM, Coppens I, Vaidya AB. 2016. Na^+ influx induced by new antimalarials causes rapid alterations in the cholesterol content and morphology of *Plasmodium falciparum*. *PLoS Pathog* **12**:e1005647. doi:10.1371/journal.ppat.1005647

Dennis ASM, Lehane AM, Ridgway MC, Holleran JP, Kirk K. 2018. Cell swelling induced by the antimalarial KAE609 (cipargamin) and other *Pf*ATP4-associated antimalarials. *Antimicrob Agents Chemother* **62**:e00087-18. doi:10.1128/AAC.00087-18

Diarra A, Sheldon C, Church J. 2001. In situ calibration and [H^+] sensitivity of the fluorescent Na^+ indicator SBFI. *American Journal of Physiology-Cell Physiology* **280**:C1623–C1633. doi:10.1152/ajpcell.2001.280.6.C1623

Eberhardt J, Santos-Martins D, Tillack AF, Forli S. 2021. AutoDock Vina 1.2.0: new docking methods, expanded force field, and python bindings. *J Chem Inf Model* **61**:3891–3898. doi:10.1021/acs.jcim.1c00203

Gray JS, Ogden NH. 2021. Ticks, human babesiosis and climate change. *Pathogens* **10**:1430. doi:10.3390/pathogens10111430

Guswanto A, Sivakumar T, Rizk MA, Elsayed SAE, Youssef MA, ElSaid EES, Yokoyama N, Igarashi I. 2014. Evaluation of a fluorescence-based method for antibabesial drug screening. *Antimicrob Agents Chemother* **58**:4713–4717. doi:10.1128/AAC.00022-14

Hidayati AR, Melinda, Ilmi H, Sakura T, Sakaguchi M, Ohmori J, Hartuti ED, Tumewu L, Inaoka DK, Tanjung M, Yoshida E, Tokumasu F, Kita K, Mori M, Dobashi K, Nozaki T, Syafruddin D, Hafid AF, Waluyo D, Widyawaruyanti A. 2023. Effect of geranylated dihydrochalcone from *Artocarpus altilis* leaves extract on *Plasmodium falciparum* ultrastructural changes and mitochondrial malate: Quinone oxidoreductase. *International Journal for Parasitology: Drugs and Drug Resistance* **21**:40–50. doi:10.1016/j.ijpddr.2022.12.001

Holbrook NR, Klontz EH, Adams GC, Schnittman SR, Issa NC, Bond SA, Branda JA, Lemieux JE. 2023. *Babesia microti* variant with multiple resistance mutations detected in an immunocompromised patient receiving atovaquone prophylaxi. *Open Forum Infectious Diseases* **10**:ofad097. doi:10.1093/ofid/ofad097

Hwang S-J, Yamasaki M, Nakamura K, Sasaki N, Murakami M, Wickramasekara Rajapakshage BK, Ohta H, Maede Y, Takiguchi M. 2010. Development and characterization of a strain of *Babesia gibsoni* resistant to diminazene aceturate *in vitro*. *J Vet Med Sci* **72**:765–771. doi:10.1292/jvms.09-0535

Jalovecka M, Sojka D, Ascencio M, Schnittger L. 2019. *Babesia* life cycle-when phylogeny meets biology. *Trends in Parasitology* **35**:356–368. doi:10.1016/j.pt.2019.01.007

569 Jeon SA, Park JL, Park S-J, Kim JH, Goh S-H, Han J-Y, Kim S-Y. 2021. Comparison
570 between MGI and Illumina sequencing platforms for whole genome sequencing. *Genes*
571 *Genom* **43**:713–724. doi:10.1007/s13258-021-01096-x
572 Ji S, Galon EM, Rizk MA, Yi Y, Zafar I, Li H, Ma Z, Iguchi A, Asada M, Liu M, Xuan X.
573 2022a. Efficacy of the antimalarial MMV390048 against *Babesia* infection reveals
574 phosphatidylinositol 4-kinase as a druggable target for babesiosis. *Antimicrob Agents*
575 *Chemother* **66**:e00574-22. doi:10.1128/aac.00574-22
576 Ji S, Liu M, Galon EM, Rizk MA, Tuvshintulga B, Li J, Zafar I, Hasegawa Y, Iguchi A,
577 Yokoyama N, Xuan X. 2022b. Inhibitory effect of naphthoquine phosphate on *Babesia*
578 *gibsoni in vitro* and *Babesia rodhaini in vivo*. *Parasites Vectors* **15**:10.
579 doi:10.1186/s13071-021-05127-0
580 Jo S, Cheng X, Islam SM, Huang L, Rui H, Zhu A, Lee HS, Qi Y, Han W, Vanommeslaeghe
581 K, MacKerell AD, Roux B, Im W. 2014. CHARMM-GUI PDB manipulator for advanced
582 modeling and simulations of proteins containing nonstandard residues. *Adv Protein Chem*
583 *Struct Biol* **96:** 235–265. doi:10.1016/bs.apcsb.2014.06.002
584 Jumper J, Evans R, Pritzel A, Green T, Figurnov M, Ronneberger O, Tunyasuvunakool K,
585 Bates R, Žídek A, Potapenko A, Bridgland A, Meyer C, Kohl SAA, Ballard AJ, Cowie A,
586 Romera-Paredes B, Nikolov S, Jain R, Adler J, Back T, et al. 2021. Highly accurate protein
587 structure prediction with AlphaFold. *Nature* **596**:583–589.
588 doi:10.1038/s41586-021-03819-2
589 Kletsova EA, Spitzer ED, Fries BC, Marcos LA. 2017. Babesiosis in Long Island: review of
590 62 cases focusing on treatment with azithromycin and atovaquone. *Ann Clin Microbiol*
591 *Antimicrob* **16**:26. doi:10.1186/s12941-017-0198-9
592 Krause PJ. 2019. Human babesiosis. *International Journal for Parasitology* **49**:165–174.
593 doi:10.1016/j.ijpara.2018.11.007
594 Krause PJ, Auwaerter PG, Bannuru RR, Branda JA, Falck-Ytter YT, Lantos PM, Lavergne V,
595 Meissner HC, Osani MC, Rips JG, Sood SK, Vannier E, Vaysbrot EE, Wormser GP. 2021.
596 Clinical practice guidelines by the infectious diseases society of America (IDSA): 2020
597 guideline on diagnosis and management of babesiosis. *Clinical Infectious Diseases*
598 **72**:e49–e64. doi:10.1093/cid/ciaa1216
599 Krause PJ, Rogers R, Shah MK, Kang H, Parsonnet J, Kodama R, Vannier E. 2024.
600 Tafenoquine for relapsing babesiosis: a case series. *Clinical Infectious Diseases*
601 **79**:130–137. doi:10.1093/cid/ciae238
602 Krishna S, Woodrow C, Webb R, Penny J, Takeyasu K, Kimura M, East JM. 2001.
603 Expression and functional characterization of a *Plasmodium falciparum* $Ca2^{+}$-ATPase
604 (*Pf*ATP4) belonging to a subclass unique to apicomplexan organisms. *Journal of*
605 *Biological Chemistry* **276**:10782–10787. doi:10.1074/jbc.M010554200
606 Lee AH, Fidock DA. 2016. Evidence of a mild mutator phenotype in cambodian *Plasmodium*

607 *falciparum* malaria parasites. *PLoS ONE* **11**:e0154166. doi:10.1371/journal.pone.0154166
608 Lehane AM, Dennis ASM, Bray KO, Li D, Rajendran E, McCoy JM, McArthur HM,
609 Winterberg M, Rahimi F, Tonkin CJ, Kirk K, Van Dooren GG. 2019. Characterization of
610 the ATP4 ion pump in *Toxoplasma gondii*. *Journal of Biological Chemistry* **294**:5720–5734.
611 doi:10.1074/jbc.RA118.006706
612 Lemieux JE, Tran AD, Freimark L, Schaffner SF, Goethert H, Andersen KG, Bazner S, Li A,
613 McGrath G, Sloan L, Vannier E, Milner D, Pritt B, Rosenberg E, Telford S, Bailey JA,
614 Sabeti PC. 2016. A global map of genetic diversity in *Babesia microti* reveals strong
615 population structure and identifies variants associated with clinical relapse. *Nat Microbiol*
616 **1**:16079. doi:10.1038/nmicrobiol.2016.79
617 Li H, Galon EM, Ji S, Zafar I, Ma Z, Do T, Amer MM, Ma Y, Liu M, Xuan X. 2023. *In vitro*
618 screening of compounds from the Food and Drug Administration-approved library
619 identifies anti-*Babesia gibsoni* activity of idarubicin hydrochloride and vorinostat.
620 *Parasitology International* **96**:102774. doi:10.1016/j.parint.2023.102774
621 Lindahl, Abraham, Hess, Spoel VD. 2021. GROMACS 2021 Manual.
622 doi:10.5281/ZENODO.4457591
623 Liu M, Adjou Moumouni PF, Cao S, Asada M, Wang G, Gao Y, Guo H, Li J, Vudriko P,
624 Efstratiou A, Ringo AE, Lee S-H, Hakimi H, Masatani T, Sunaga F, Kawazu S, Yamagishi
625 J, Jia L, Inoue N, Xuan X. 2018. Identification and characterization of interchangeable
626 cross-species functional promoters between *Babesia gibsoni* and *Babesia bovis*. *Ticks and*
627 *Tick-borne Diseases* **9**:330–333. doi:10.1016/j.ttbdis.2017.11.008
628 Liu M, Ji S, Kondoh D, Galon EM, Li J, Tomihari M, Yanagawa M, Tagawa M, Adachi M,
629 Asada M, Igarashi I, Iguchi A, Xuan X. 2021. Tafenoquine is a promising drug candidate
630 for the treatment of babesiosis. *Antimicrob Agents Chemother* **65**:e00204-21.
631 doi:10.1128/AAC.00204-21
632 Marcos LA, Leung A, Kirkman L, Wormser GP. 2022. Use of tafenoquine to treat a patient
633 with relapsing babesiosis with clinical and molecular evidence of resistance to
634 azithromycin and atovaquone. *IDCases* **27**:e01460. doi:10.1016/j.idcr.2022.e01460
635 Matsuu A, Koshida Y, Kawahara M, Inoue K, Ikadai H, Hikasa Y, Okano S, Higuchi S. 2004.
636 Efficacy of atovaquone against *Babesia gibsoni in vivo* and *in vitro*. *Veterinary*
637 *Parasitology* **124**:9-18. doi:10.1016/j.vetpar.2004.07.005
638 Mohring F, Van Schalkwyk DA, Henrici RC, Blasco B, Leroy D, Sutherland CJ, Moon RW.
639 2022. Cation ATPase (ATP4) orthologue replacement in the malaria parasite *Plasmodium*
640 *knowlesi* reveals species-specific responses to ATP4-targeting drugs. *mBio* **13**:e01178-22.
641 doi:10.1128/mbio.01178-22
642 Mordue DG, Wormser GP. 2019. Could the drug tafenoquine revolutionize treatment of
643 *Babesia microti* infection? *J Infect Dis* **220**:442-447. doi: 10.1093/infdis/jiz119
644 Ndayisaba G, Yeka A, Asante KP, Grobusch MP, Karita E, Mugerwa H, Asiimwe S, Oduro A,

645 Fofana B, Doumbia S, Jain JP, Barsainya S, Kullak-Ublick GA, Su G, Schmitt EK,
646 Csermak K, Gandhi P, Hughes D. 2021. Hepatic safety and tolerability of cipargamin
647 (KAE609), in adult patients with *Plasmodium falciparum* malaria: a randomized, phase II,
648 controlled, dose-escalation trial in sub-Saharan Africa. *Malar J* **20**:478.
649 doi:10.1186/s12936-021-04009-1
650 Qiu D, Pei JV, Rosling JEO, Thathy V, Li D, Xue Y, Tanner JD, Penington JS, Aw YTV, Aw
651 JYH, Xu G, Tripathi AK, Gnadig NF, Yeo T, Fairhurst KJ, Stokes BH, Murithi JM,
652 Kümpornsin K, Hasemer H, Dennis ASM, et al. 2022. A G358S mutation in the
653 *Plasmodium falciparum* Na^+ pump *Pf*ATP4 confers clinically-relevant resistance to
654 cipargamin. *Nat Commun* **13**:5746. doi:10.1038/s41467-022-33403-9
655 Qurollo BA, Archer NR, Schreeg ME, Marr HS, Birkenheuer AJ, Haney KN, Thomas BS,
656 Breitschwerdt EB. 2017. Improved molecular detection of *Babesia* infections in animals
657 using a novel quantitative real-time PCR diagnostic assay targeting mitochondrial DNA.
658 *Parasites Vectors* **10**:128. doi:10.1186/s13071-017-2064-1
659 Rogers R, Krause PJ, Norris AM, Ting MH, Nagami EH, Cilley B, Vannier E. 2023. Broad
660 antimicrobial resistance in a case of relapsing babesiosis successfully treated with
661 tafenoquine. *Clinical Infectious Diseases* **76**:741–744. doi:10.1093/cid/ciac473
662 Rosenblatt J, Leung A, Baneman E, Fuller R, Taimur S, Paniz-Mondolfi AE, Malone AK,
663 Kirkman L, Jacobs SE. 2021. Relapsed *Babesia microti* infection following allogeneic
664 hematopoietic cell transplantation in a patient with B-cell acute lymphoblastic leukemia:
665 case report and review of the literature. *Open Forum Infectious Diseases* **8**:ofab323.
666 doi:10.1093/ofid/ofab323
667 Rosling JEO, Ridgway MC, Summers RL, Kirk K, Lehane AM. 2018. Biochemical
668 characterization and chemical inhibition of *Pf*ATP4-associated Na^+-ATPase activity in
669 *Plasmodium falciparum* membranes. *Journal of Biological Chemistry* **293**:13327–13337.
670 doi:10.1074/jbc.RA118.003640
671 Rottmann M, McNamara C, Yeung BKS, Lee MCS, Zou B, Russell B, Seitz P, Plouffe DM,
672 Dharia NV, Tan J, Cohen SB, Spencer KR, González-Páez GE, Lakshminarayana SB, Goh
673 A, Suwanarusk R, Jegla T, Schmitt EK, Beck H-P, Brun R, et al. 2010. Spiroindolones, a
674 potent compound class for the treatment of malaria. *Science* **329**:1175–1180.
675 doi:10.1126/science.1193225
676 Saliba KJ, Kirk K. 1999. pH regulation in the intracellular malaria parasite, *Plasmodium*
677 *falciparum*. *Journal of Biological Chemistry* **274**:33213–33219.
678 doi:10.1074/jbc.274.47.33213
679 Schmitt EK, Ndayisaba G, Yeka A, Asante KP, Grobusch MP, Karita E, Mugerwa H, Asiimwe
680 S, Oduro A, Fofana B, Doumbia S, Su G, Csermak Renner K, Venishetty VK, Sayyed S,
681 Straimer J, Demin I, Barsainya S, Boulton C, Gandhi P. 2022. Efficacy of cipargamin
682 (KAE609) in a randomized, phase II dose-escalation study in adults in Sub-Saharan Africa

683 with uncomplicated *Plasmodium falciparum* malaria. *Clinical Infectious Diseases*
684 **74**:1831–1839. doi:10.1093/cid/ciab716
685 Simon MS, Westblade LF, Dziedziech A, Visone JE, Furman RR, Jenkins SG, Schuetz AN,
686 Kirkman LA. 2017. Clinical and molecular evidence of atovaquone and azithromycin
687 resistance in relapsed *Babesia microti* infection associated with rituximab and chronic
688 lymphocytic leukemia. *Clinical Infectious Diseases* **65**:1222–1225. doi:10.1093/cid/cix477
689 Spillman NJ, Allen RJW, McNamara CW, Yeung BKS, Winzeler EA, Diagana TT, Kirk K.
690 2013. Na^+ regulation in the malaria parasite *Plasmodium falciparum* involves the cation
691 ATPase *Pf*ATP4 and is a target of the spiroindolone antimalarials. *Cell Host & Microbe*
692 **13**:227–237. doi:10.1016/j.chom.2012.12.006
693 Tayebwa DS, Tuvshintulga B, Guswanto A, Nugraha AB, Batiha GE-S, Gantuya S, Rizk MA,
694 Vudriko P, Sivakumar T, Yokoyama N, Igarashi I. 2018. The effects of nitidine chloride
695 and camptothecin on the growth of *Babesia* and *Theileria* parasites. *Ticks and Tick-borne*
696 *Diseases* **9**:1192–1201. doi:10.1016/j.ttbdis.2018.04.019
697 Trott O, Olson AJ. 2010. AutoDock Vina: improving the speed and accuracy of docking with
698 a new scoring function, efficient optimization, and multithreading. *J Comput Chem*
699 **31**:455–461. doi:10.1002/jcc.21334
700 Tuvshintulga B, Sivakumar T, Nugraha AB, Ahedor B, Batmagnai E, Otgonsuren D, Liu M,
701 Xuan X, Igarashi I, Yokoyama N. 2022. Combination of clofazimine and atovaquone as a
702 potent therapeutic regimen for the radical cure of *Babesia microti* infection in
703 immunocompromised hosts. *The Journal of Infectious Diseases* **225**:238–242.
704 doi:10.1093/infdis/jiab537
705 Vannier E, Krause PJ. 2012. Human babesiosis. *N Engl J Med* **366**:2397–2407.
706 doi:10.1056/NEJMra1202018
707 Vega CA, Buening GM, Green TJ, Carson CA. 1985. *In vitro* cultivation of *Babesia bigemina*.
708 *Am J Vet Res* **46**:416–420.
709 Vydyam P, Pal AC, Renard I, Chand M, Kumari V, Gennaro JC, Mamoun CB. 2024.
710 Tafenoquine-atovaquone combination achieves radical cure and confers sterile immunity in
711 experimental models of human babesiosis. *The Journal of Infectious Diseases*
712 **229**:161–172. doi:10.1093/infdis/jiad315
713 Zhang R, Suwanarusk R, Malleret B, Cooke BM, Nosten F, Lau Y-L, Dao M, Lim CT, Renia
714 L, Tan KSW, Russell B. 2016. A basis for rapid clearance of circulating ring-stage malaria
715 parasites by the spiroindolone KAE609. *J Infect Dis* **213**:100–104.
716 doi:10.1093/infdis/jiv358
717 Zhou Y, Fomovska A, Muench S, Lai B-S, Mui E, McLeod R. 2014. Spiroindolone that
718 inhibits *Pf*ATPase4 is a potent, cidal inhibitor of *Toxoplasma gondii* tachyzoites *in vitro*
719 and *in vivo*. *Antimicrob Agents Chemother* **58**:1789–1792. doi:10.1128/AAC.02225-13
720

721 **Figure Legends**

722 **Figure 1. CIP demonstrates potent inhibition on *Babesia* spp. (A)** and (**B)** Dose-dependent
723 growth curve of CIP on *B. bovis* and *B. gibsoni in vitro*. Each value represents the mean ±
724 standard deviation (SD) of three independent experiments carried out in triplicate. IC_{50}: the
725 half maximal inhibitory concentration. (**C)** Inhibitory effects of CIP and atovaquone (ATO)
726 plus azithromycin (AZI) on the proliferation of *B. microti* in BALB/c mice. (**D)** Hematocrit
727 (HCT) values in mice treated with CIP or ATO plus AZI compared with vehicle-treated mice.
728 (**E)** Inhibitory effects of CIP and ATO plus AZI on the proliferation of *B. rodhaini* in BALB/c
729 mice. (**F)** Survival rates of CIP-treated, ATO plus AZI-treated, and vehicle-treated mice. The
730 treatment time is shown by two-way arrows, and significant differences ($P < 0.01$) between
731 the drug-treated groups and the vehicle-treated control group are indicated by asterisks. The
732 data from one of six individual experiments are expressed as means ± SD. **, $P < 0.01$.

733

734 **Figure 2. Mutations in BgATP4 mediate CIP resistance. (A-C)** Representative sequencing
735 chromatogram of wild-type and resistant parasites from CIP-treated *B. gibsoni*. The resistant
736 parasite genomic DNA is extracted from blood samples after a 60 day-treatment. The
737 BgATP4 gene was amplified and sequenced using the DNA. (**D)** Genes of high-frequency
738 sequence variants detected by NGS. (**E)** Dose-dependent growth curve of $BgATP4^{WT}$,
739 $BgATP4^{L921V}$, and $BgATP4^{L921I}$ *in vitro*. Each value represents the mean ± standard deviation
740 (SD) of three independent experiments carried out in triplicate.

741

742 **Figure 3. Mechanistic basis for resistance to CIP conferred by the L921V and L921I**
743 **mutations in BgATP4. (A)** Untreated and CIP-treated parasite morphology after incubation
744 for 72 h. Scale bar: 5 μm. (**B)** Sizes of 100 parasites in two groups measured with ImageJ

745 software in panels A. Statistically significant differences between the means of variables
746 determined by t-test. ****, $P < 0.0001$. (**C**) TEM of untreated and CIP-treated parasite. N,
747 Nucleus; SB, spherical body; V, vacuole. Scale bar: 500 nm. (**D**) $[Na^+]_i$ concentrations after
748 the addition of CIP in the BgATP4^{WT} line. Representative traces from the experiment that
749 highlight the impact of adding 20 nM CIP (blue), 1 nM CIP (green), or 0 nM CIP (grey) on
750 the concentration $[Na^+]_i$ of the BgATP4^{WT} line. (**E**) Alkalinization of pH_i in BgATP4^{WT} line
751 upon addition of the ATP4 inhibitor. (**F**) Addition of 20 nM CIP to the wild-type and resistant
752 parasite lines results in different $[Na^+]_i$ concentrations. (**G**) Addition of 20 nM CIP to the
753 wild-type and resistant parasite lines results in different pH_i concentrations. Experiments were
754 performed in technical duplicates for at least three biological repeats. **(H)** Data acquired in
755 the low Na^+ condition (containing only the 2 mM Na^+ introduced upon the addition of 1 mM
756 Na_2ATP) was subtracted from data obtained in the high Na^+ condition to determine the
757 ATPase activity related to the BgATP4 proteins. The results are presented as the average of
758 data from three independent tests. (**I**) Dose-dependent BgATP4-associated ATPase activity
759 curve of BgATP4^{WT}, BgATP4^{L921V}, and BgATP4^{L921I} *in vitro*. ATPase activity was determined
760 at pH 7.2 in the presence of 150 mM Na^+ and 1 mM Na_2ATP. Each value represents the mean
761 ± standard deviation (SD) of three independent experiments carried out in triplicate. *, $P <$
762 0.05; **, $P < 0.01$.
763

764 **Figure 4. Binding sites proximal to BgATP4 residue 921 predicted by molecular docking.**
765 **(A)** The lowest energy poses for CIP were located in reference to the whole protein structure,
766 docking against the WT (green), L921V (yellow), and L921I (pink) mutant BgATP4. The side
767 chain of L921 is also shown in a red stick at its position. (**B-D**) The zoomed views of the
768 binding locations of CIP.
769

770 **Figure 5. Cross-resistance between ATO and TQ in resistant parasites and combination**
771 **therapy based on CIP plus TQ. (A)** Dose-dependent growth curve of BgATP4^{WT},
772 BgATP4^{L921V}, and BgATP4^{L921I} by ATO treatment *in vitro*. **(B)** Dose-dependent growth curve
773 of BgATP4^{WT}, BgATP4^{L921V}, and BgATP4^{L921I} by TQ treatment *in vitro.* Each value
774 represents the mean ± standard deviation (SD) of three independent experiments carried out
775 in triplicate. **(C)** Inhibitory effects of CIP plus TQ on the proliferation of *B. microti* in SCID
776 mice. Treatment started at 4 DPI: CIP was given at 20 mg/kg once daily for 7 days, TQ was
777 administered as a single 20 mg/kg dose, and the combination group received both treatments
778 (CIP at 20 mg/kg once daily for 7 days plus a single dose of TQ at 20 mg/kg). The data are
779 presented as the means from one of five independent experiments. **(D)** Parasite DNA was
780 detected by qPCR on genomic DNA extracted from blood collected from untreated and
781 treated SCID mice infected with *B. microti* at 90 DPI. A dotted grey line across the graph
782 represents the average cut-off Cq value. Cut-off Cq ≤ 35 was considered positive, while Cq >
783 35 or no amplification was considered negative. Each sample was analyzed in duplicate, and
784 two independent experiments were conducted. NA indicates no amplification.

785 **Supplementary Materials**

786 **Figure supplement 1. Cytotoxicity assay of CIP on the Madin-Darby canine kidney**
787 **(MDCK) cells and human foreskin fibroblasts (HFF).** The MTP-500 microplate reader
788 was utilized to detect the absorbance at 450 nm. The results are displayed as the mean ±
789 standard deviation of three separate tests. CC_{50}: the 50% cytotoxic concentration.

790

791 **Figure supplement 2. Multiple sequence alignment of ATP4 in different species.** A
792 yellow square and arrow denotes the BgATP4 mutation site discovered in this investigation;
793 purple squares and arrows represent sites linked to *P. falciparum* CIP resistance, and a gray
794 square and arrow represent sites associated with *T. gondii*.

795

796 **Figure supplement 3. Binding sites for CIP found by Gnina search across the entire**
797 **surface of the protein.** (**A-C**) The binding space of WT, L921V, and L921I mutants in
798 BgATP4 are labeled in green, yellow, and pink, respectively.

799

800 **Figure supplement 4. Proposed mechanism of inhibition of CIP on wild-type and mutant**
801 **parasite-infected erythrocytes.** CIP disrupts the BgATP4 function of wild-type parasites,
802 which causes a net influx of Na^+ and efflux of H^+ from the parasite. The osmotic load
803 imposed on the influx of Na^+ further brings about parasite swelling and internal alkalinization,
804 which are the main factors in *Babesia* death. Mutations in ATP4 minimize the susceptibility
805 to ATP4 inhibitors by recovering H^+ and Na^+ balance, as indicated by the dotted arrows.

806 **Supplemental Tables**

807 **Table supplement 1.** Primer sets of *B. gibsoni* ATP4

Gene	Primer (5'-3')
Bgatp4-1F	ACGTAGTTGTCGAACATCTTACACCAATGC
Bgatp4-1R	CAGAGGTAGCATAGTGAGATCGCCCCGA
Bgatp4-2F	GAGATTGCAAGGTTTACGGATGAGTCTATGG
Bgatp4-2R	ATGACAACGTCACCGGGTACAACACGCTTG
Bgatp4-3F	GAAAAGCTTGCTCAAATGTCTTCACCGACAAC
Bgatp4-3R	GTTTCTGGACGAGTTGGATCCTCATAACC
Bgatp4-4F	AAATTGGGGGGGATAATTGGCATTATCTCC
Bgatp4-4R	ACCTTATCAAAGGGTACCTCTTGCTTTG
Bgatp4-5F	TCAATCCATTCGGTGGAATTTTCAAAAAGG
Bgatp4-5R	GTGTTTGAATAACATATCTGGTGCCCCCTT
Bgatp4-6F	GGTAAAGAACAGATTTGCTGACATAGATCT
Bgatp4-6R	ACCCTATTTCTTGTGCGATGGCCGTAGCTG
Bgatp4-7F	AGGGACGCTATAAATACTTGTGGAAAGGC
Bgatp4-7R	GTACGCCCAGACTCGATTGAGTTAACTATTG
Bgatp4-8F	GGGTATTAATGGCACAGATGTTGCAAAAGG
Bgatp4-8R	GACAGTTCCCACTAGCATCATTAAGTGTAA
Bgatp4-9F	ATCATCATTGCGCTATATGTTTCTACCGG
Bgatp4-9R	CTAATGGGGTAGCATTTCCATTCTCAACAA
Bgatp4-10F	AGGGAGTTCCTCCCATGTATAAAGATACCT
Bgatp4-10R	TTAGGCTTCTGCCCTTTTCATTTTTCGCTT

808

809 **Table supplement 2.** Primer sets of *B. microti* ATP4

Gene	Primer (5'-3')
Bmatp4-1F	ATGAGTAGATCTCAGTCTAACATTTC
Bmatp4-1R	TGCTATTAGTAGTGCTATAACAAAG
Bmatp4-2F	CAAGTATGGCGAAAATGCTATAAAC
Bmatp4-2R	CATTCCGTTTGTTACGCTGGTGC
Bmatp4-3F	CTTACAGGTGAGAGTGAAGATGTAAAG
Bmatp4-3R	ACAAATTGCTGAGCAGCAACCCAGAG
Bmatp4-4F	CTATTTCATTGTCATTGGGAGCTAA
Bmatp4-4R	CAAATCCGGCCTTAGCTGCGCCAA
Bmatp4-5F	TCATACGGTTCAACGTTATCACATG
Bmatp4-5R	TCTATCCGACGACTCCAACCTTTC
Bmatp4-6F	GTTGTCCAAGAATGCTTATAGGGTG
Bmatp4-6R	CATTGCCACGCCAATGTCCGCCTGTTT
Bmatp4-7F	GTTAACTCGTTGAAGAGACAAGGTTAC
Bmatp4-7R	CACAATTGTACCGACAACTGCCGCTG
Bmatp4-8F	GGCCAAAATCTCAGCCTTTAATGAC
Bmatp4-8R	CAGCTCCAATGGGTTGGTAGTAACCATT
Bmatp4-9F	CGTTATTGACGGCGTTGAGAATGATG
Bmatp4-9R	CCCAAAACACCTTTGCCATTTAACTC
Bmatp4-10F	GAAAATTGTAGAGCATTTCAAAACCAG
Bmatp4-10R	TTATTGCAGGGCAGCCTGCTTAGA

810

811 **Table supplement 3.** Interactions of CIP from docking simulations

Receptor and binding energy	Name	Distance	Category	Types
BgATP4^{WT} -6.43 kcal/mol	GLY407	2.67648	Hydrogen Bond; Halogen	Carbon Hydrogen Bond; Halogen (Fluorine)
	CYS959	3.2396	Halogen	Halogen (Cl, Br, I)
	VAL962	2.66882	Hydrophobic	Pi-Sigma
	CYS959	4.38742	Hydrophobic	Alkyl
	VAL962	4.29249	Hydrophobic	Alkyl
	ALA963	3.8231	Hydrophobic	Alkyl
	ALA1202	3.67015	Hydrophobic	Alkyl
	MET211	5.06565	Hydrophobic	Alkyl
	VAL962	4.25668	Hydrophobic	Alkyl
	ILE414	4.70605	Hydrophobic	Alkyl
	CYS959	4.83891	Hydrophobic	Pi-Alkyl
	VAL962	4.98402	Hydrophobic	Pi-Alkyl
	VAL411	5.43239	Hydrophobic	Pi-Alkyl
	VAL962	5.05537	Hydrophobic	Pi-Alkyl
	PHE954	4.07586	Hydrophobic	Pi-Alkyl
BgATP4^{L921V} -6.40 kcal/mol	GLY407	2.69013	Hydrogen Bond; Halogen	Carbon Hydrogen Bond; Halogen (Fluorine)
	CYS959	3.22066	Halogen	Halogen (Cl, Br, I)
	VAL962	2.66391	Hydrophobic	Pi-Sigma
	CYS959	4.35422	Hydrophobic	Alkyl
	VAL962	4.31879	Hydrophobic	Alkyl
	ALA963	3.8209	Hydrophobic	Alkyl
	ALA1202	3.63038	Hydrophobic	Alkyl
	MET211	5.0878	Hydrophobic	Alkyl
	VAL962	4.24186	Hydrophobic	Alkyl
	ILE414	4.71819	Hydrophobic	Alkyl
	CYS959	4.82036	Hydrophobic	Pi-Alkyl
	VAL962	4.99879	Hydrophobic	Pi-Alkyl
	VAL411	5.4334	Hydrophobic	Pi-Alkyl
	VAL962	5.04532	Hydrophobic	Pi-Alkyl
	PHE954	4.07482	Hydrophobic	Pi-Alkyl
	GLY958	2.92346	Hydrogen Bond; Halogen	Carbon Hydrogen Bond; Halogen (Fluorine)
	GLY958	3.3301	Halogen	Halogen (Fluorine)
	MET410	5.88505	Other	Pi-Sulfur

	VAL955	4.31406	Hydrophobic	Alkyl
	MET410	3.69023	Hydrophobic	Alkyl
$BgATP4^{L921I}$	VAL411	4.83101	Hydrophobic	Alkyl
-6.26 kcal/mol	VAL955	4.79513	Hydrophobic	Alkyl
	VAL955	4.84729	Hydrophobic	Alkyl
	CYS959	4.1269	Hydrophobic	Alkyl
	ILE1205	4.82529	Hydrophobic	Alkyl
	CYS959	5.21399	Hydrophobic	Alkyl
	VAL955	4.90527	Hydrophobic	Pi-Alkyl
	PHE954	5.03012	Hydrophobic	Pi-Alkyl

812

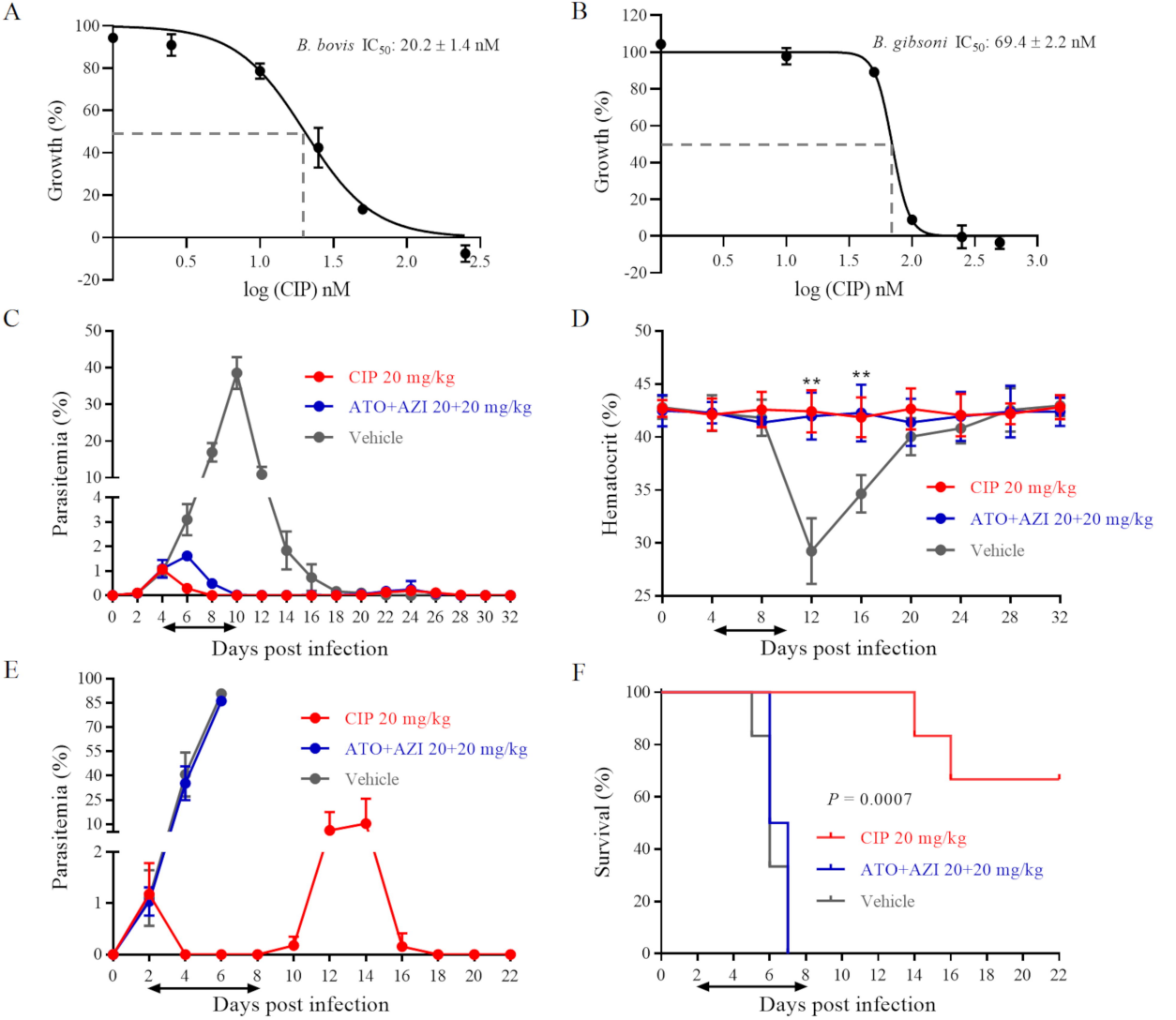
A
B. bovis IC50: 20.2 ± 1.4 nM
Growth (%)
log (CIP) nM
B
B. gibsoni IC50: 69.4 ± 2.2 nM
Growth (%)
log (CIP) nM
C
Parasitemia (%)
CIP 20 mg/kg
ATO+AZI 20+20 mg/kg
Vehicle
Days post infection
D
Hematocrit (%)
**
**
CIP 20 mg/kg
ATO+AZI 20+20 mg/kg
Vehicle
Days post infection
E
Parasitemia (%)
CIP 20 mg/kg
ATO+AZI 20+20 mg/kg
Vehicle
Days post infection
F
Survival (%)
P = 0.0007
CIP 20 mg/kg
ATO+AZI 20+20 mg/kg
Vehicle
Days post infection

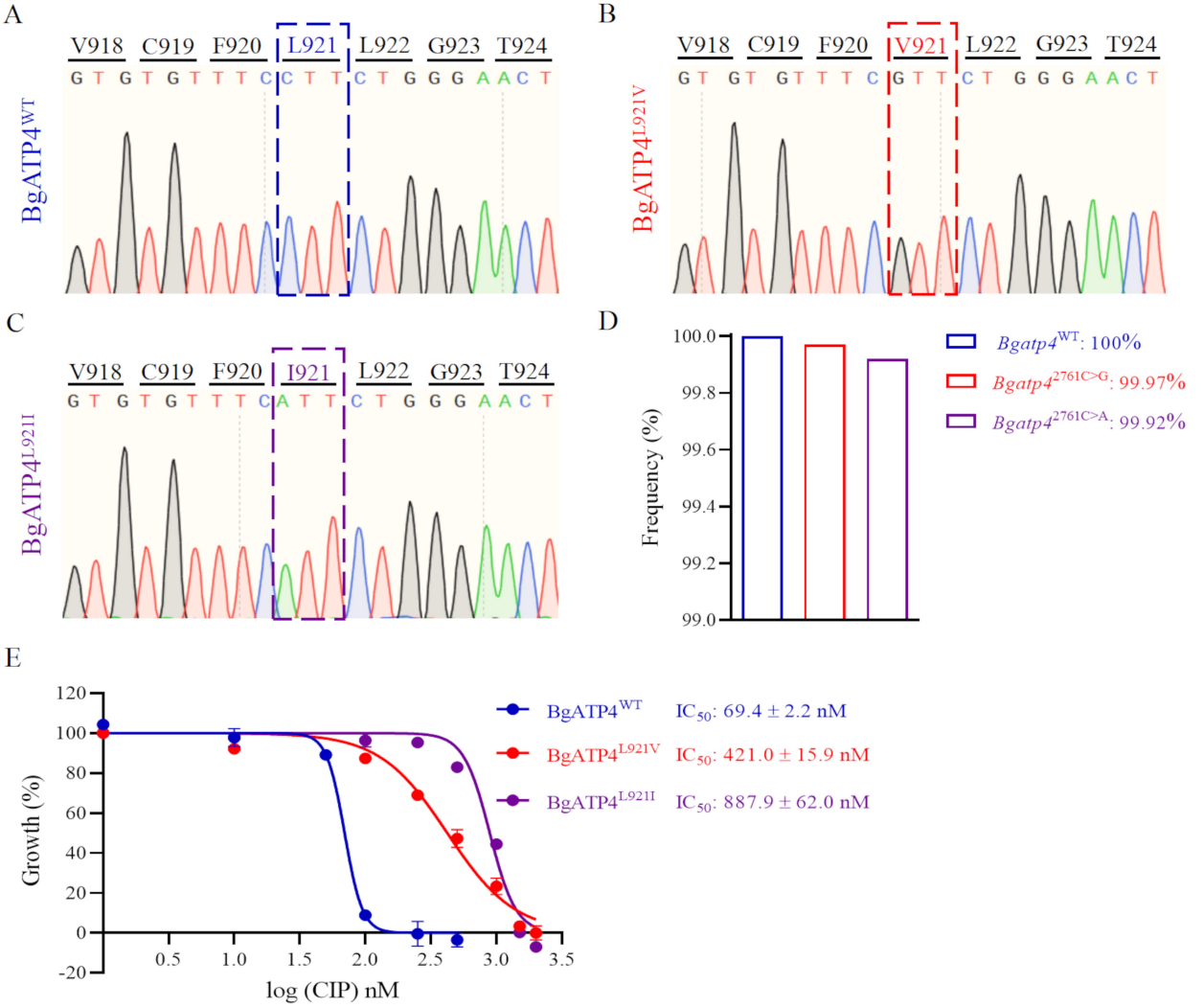
A
V918 C919 F920 L921 L922 G923 T924
G T G T G T T T C C T T C T G G G A A C T
BgATP4WT
B
V918 C919 F920 V921 L922 G923 T924
G T G T G T T T C G T T C T G G G A A C T
BgATP4L921V
C
V918 C919 F920 I921 L922 G923 T924
G T G T G T T T C A T T C T G G G A A C T
BgATP4L921I
D
Frequency (%)
100.0
99.8
99.6
99.4
99.2
99.0
Bgatp4WT: 100%
Bgatp4 2761C>G: 99.97%
Bgatp4 2761C>A: 99.92%
E
Growth (%)
120
100
80
60
40
20
0
-20
0.5
1.0
1.5
2.0
2.5
3.0
3.5
log (CIP) nM
BgATP4WT IC50: 69.4 ± 2.2 nM
BgATP4L921V IC50: 421.0 ± 15.9 nM
BgATP4L921I IC50: 887.9 ± 62.0 nM

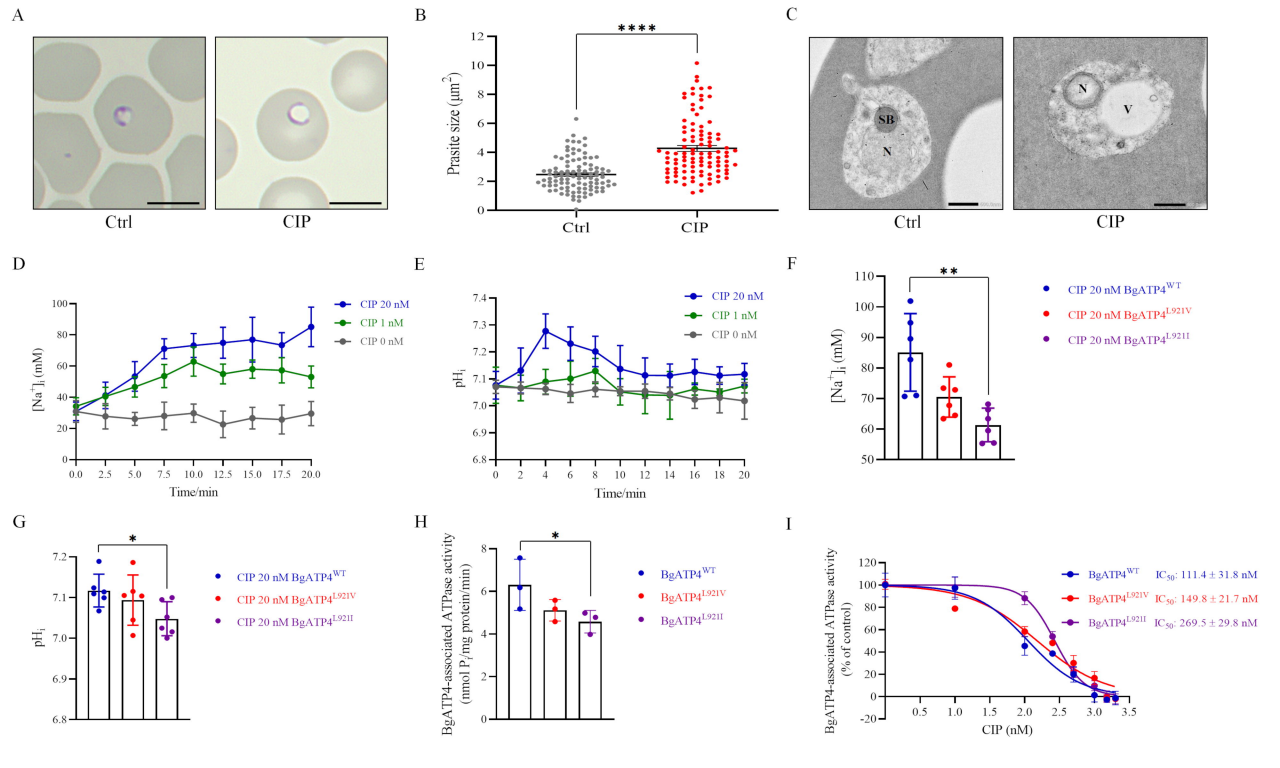
A
Ctrl
CIP
B
****
Prasite size (μm²)
Ctrl
CIP
C
SB
N
N
V
Ctrl
CIP
D
[Na⁺]i (mM)
Time/min
CIP 20 nM
CIP 1 nM
CIP 0 nM
E
pHi
Time/min
CIP 20 nM
CIP 1 nM
CIP 0 nM
F
**
[Na⁺]i (mM)
CIP 20 nM BgATP4WT
CIP 20 nM BgATP4L921V
CIP 20 nM BgATP4L921I
G
*
pHi
CIP 20 nM BgATP4WT
CIP 20 nM BgATP4L921V
CIP 20 nM BgATP4L921I
H
*
BgATP4-associated ATPase activity (nmol Pi/mg protein/min)
BgATP4WT
BgATP4L921V
BgATP4L921I
I
BgATP4-associated ATPase activity (% of control)
CIP (nM)
BgATP4WT IC50: 111.4 ± 31.8 nM
BgATP4L921V IC50: 149.8 ± 21.7 nM
BgATP4L921I IC50: 269.5 ± 29.8 nM

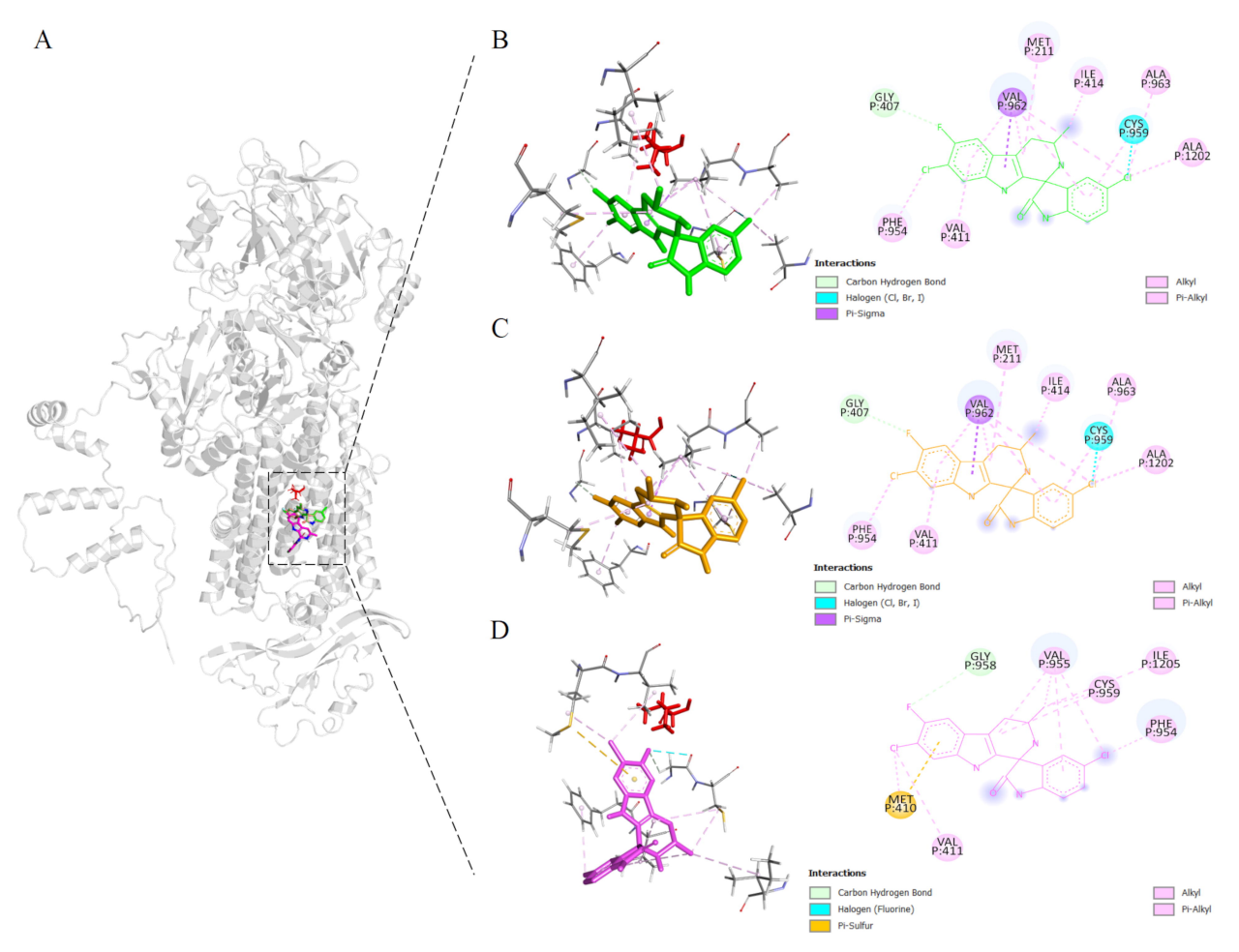
A
B
MET P:211
ILE P:414
ALA P:963
GLY P:407
VAL P:962
CYS P:959
ALA P:1202
PHE P:954
VAL P:411
Interactions
Carbon Hydrogen Bond
Halogen (Cl, Br, I)
Pi-Sigma
Alkyl
Pi-Alkyl
C
MET P:211
ILE P:414
ALA P:963
GLY P:407
VAL P:962
CYS P:959
ALA P:1202
PHE P:954
VAL P:411
Interactions
Carbon Hydrogen Bond
Halogen (Cl, Br, I)
Pi-Sigma
Alkyl
Pi-Alkyl
D
GLY P:958
VAL P:955
ILE P:1205
CYS P:959
PHE P:954
MET P:410
VAL P:411
Interactions
Carbon Hydrogen Bond
Halogen (Fluorine)
Pi-Sulfur
Alkyl
Pi-Alkyl

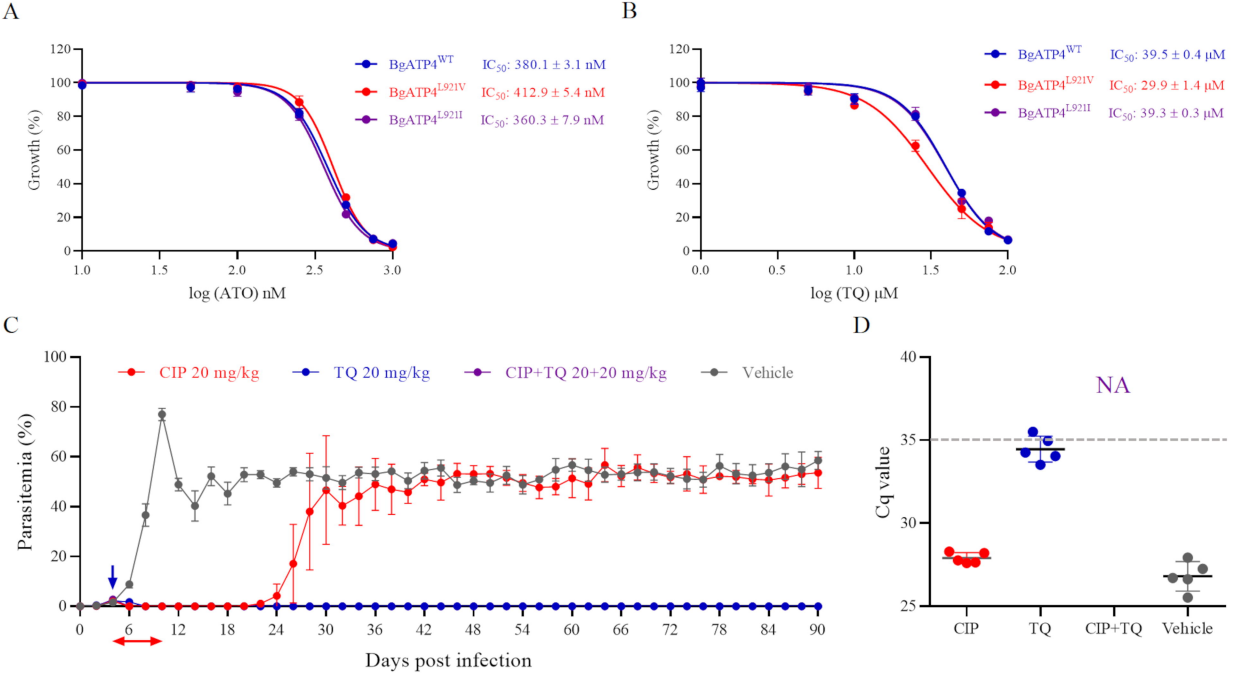
A
Growth (%)
log (ATO) nM
BgATP4WT IC50: 380.1 ± 3.1 nM
BgATP4L921V IC50: 412.9 ± 5.4 nM
BgATP4L921I IC50: 360.3 ± 7.9 nM
B
Growth (%)
log (TQ) μM
BgATP4WT IC50: 39.5 ± 0.4 μM
BgATP4L921V IC50: 29.9 ± 1.4 μM
BgATP4L921I IC50: 39.3 ± 0.3 μM
C
CIP 20 mg/kg
TQ 20 mg/kg
CIP+TQ 20+20 mg/kg
Vehicle
Parasitemia (%)
Days post infection
D
NA
Cq value
CIP
TQ
CIP+TQ
Vehicle

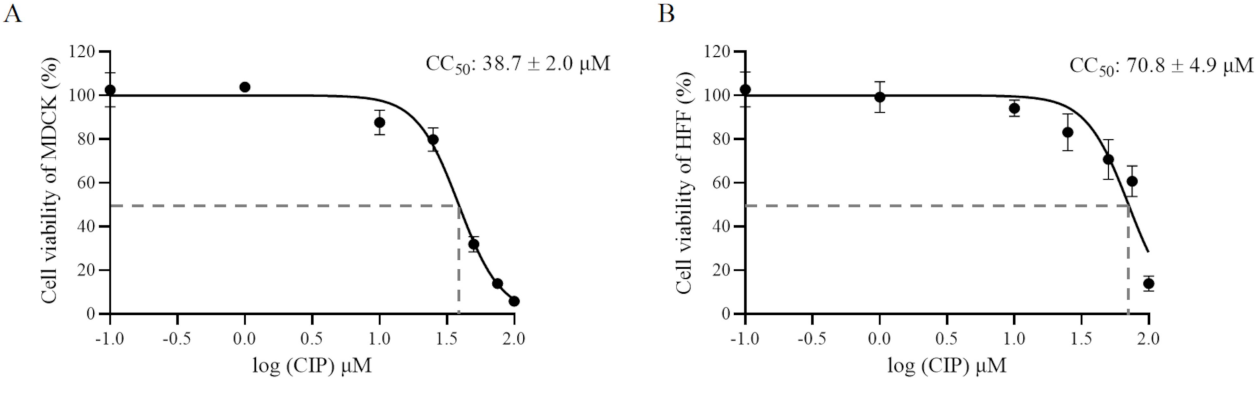
A
CC50: 38.7 ± 2.0 μM
Cell viability of MDCK (%)
120
100
80
60
40
20
0
-1.0
-0.5
0.0
0.5
1.0
1.5
2.0
log (CIP) μM
B
CC50: 70.8 ± 4.9 μM
Cell viability of HFF (%)
120
100
80
60
40
20
0
-1.0
-0.5
0.0
0.5
1.0
1.5
2.0
log (CIP) μM

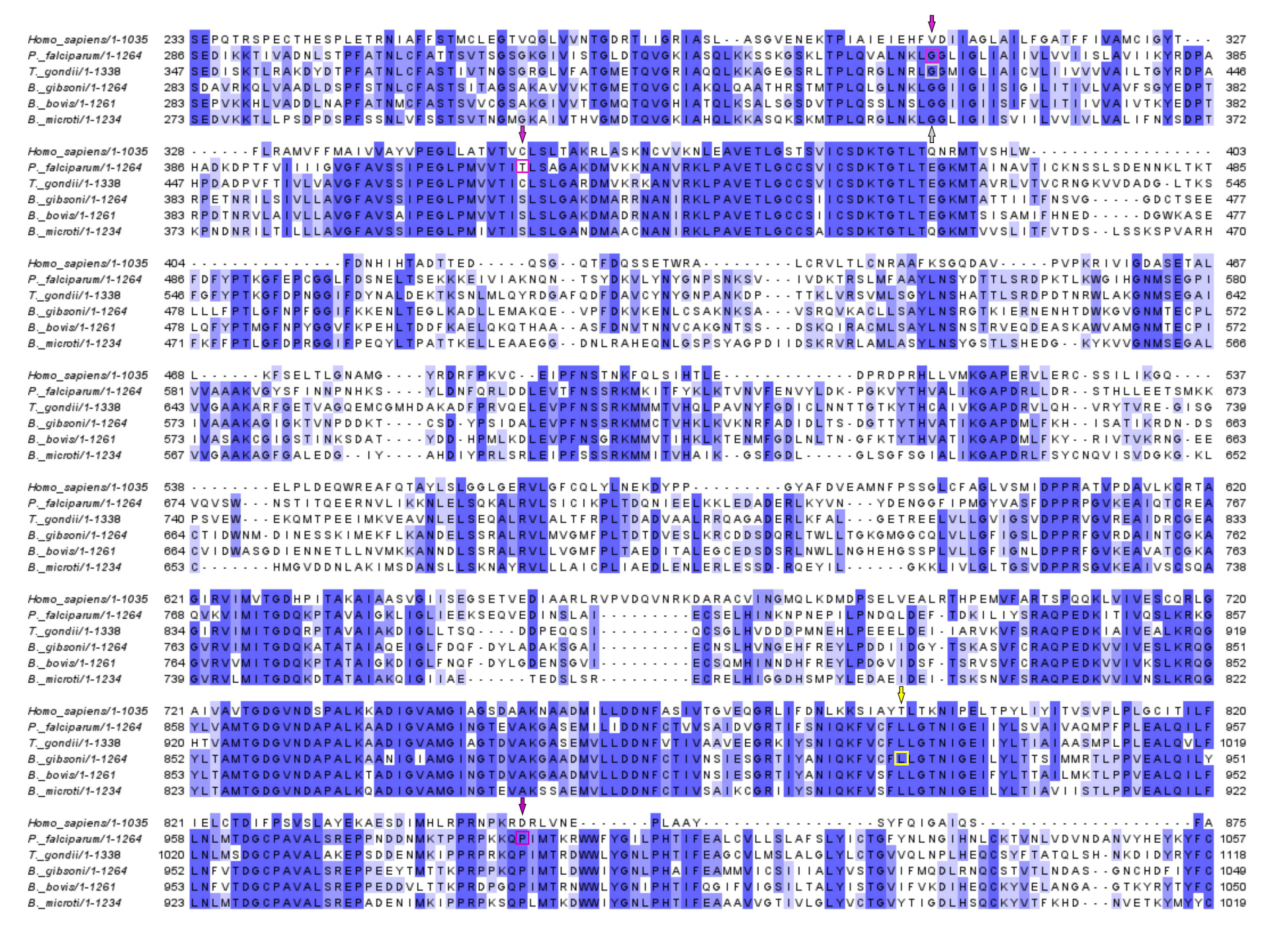
Homo_sapiens/1-1035
P._falciparum/1-1264
T._gondii/1-1338
B._gibsonii/1-1264
B._bovis/1-1261
B._microti/1-1234

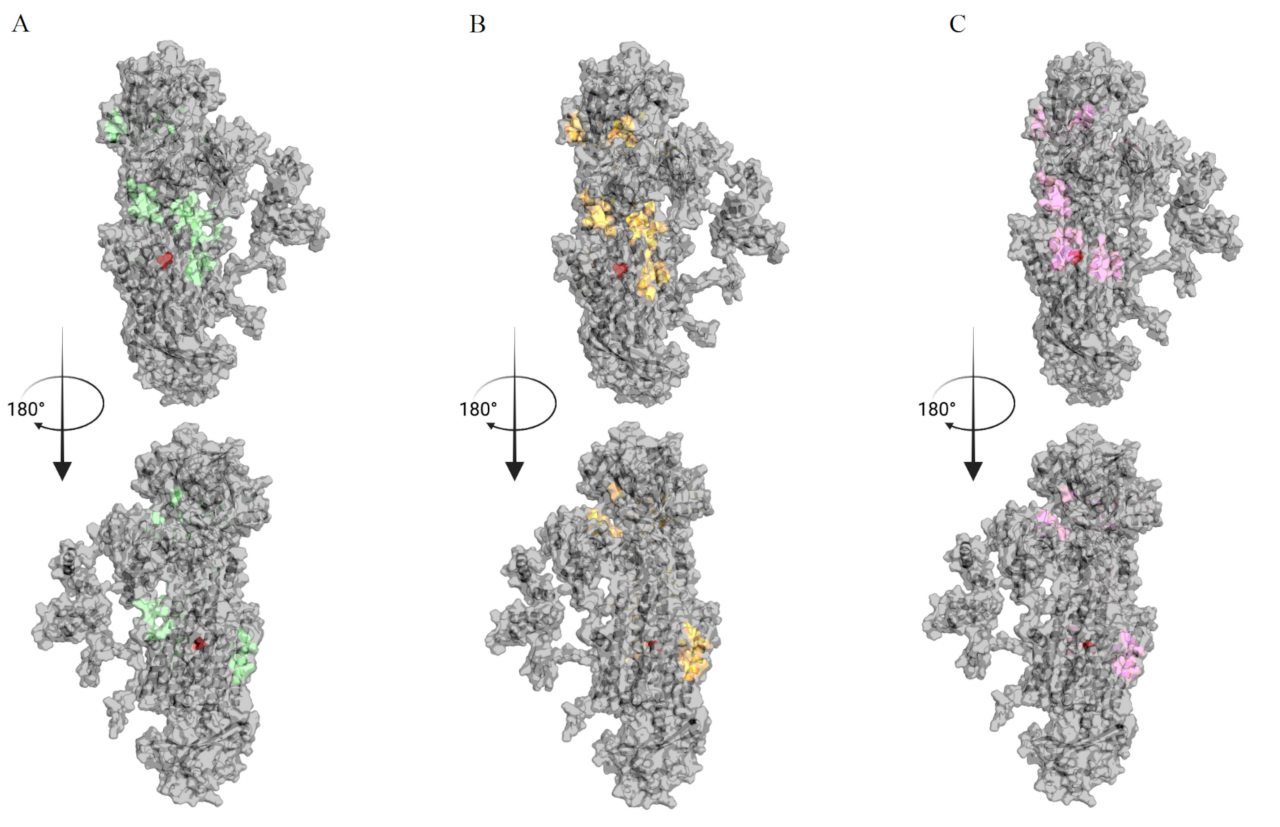
A
180°
B
180°
C
180°

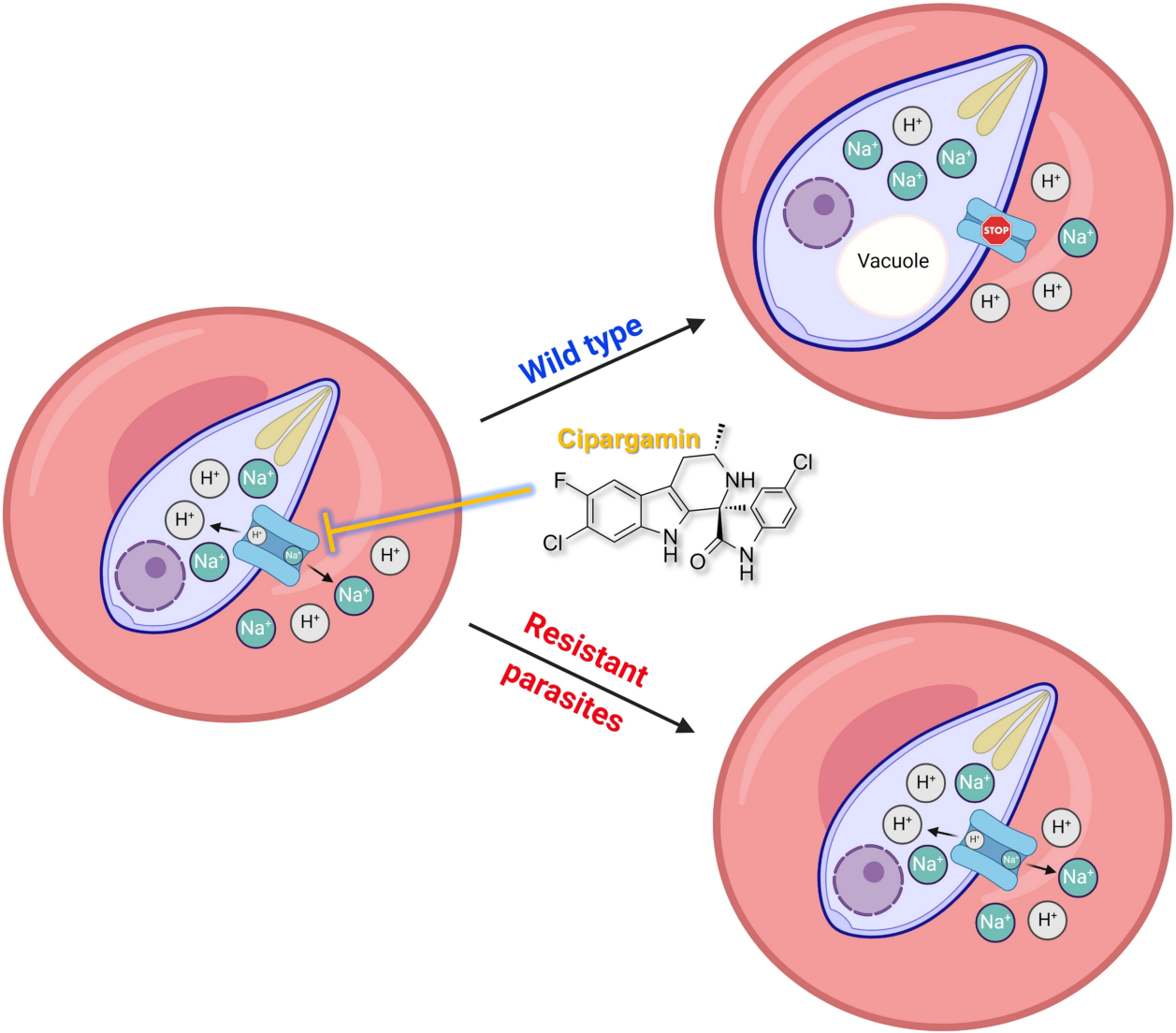
Wild type
Cipargamin
Resistant parasites
Vacuole
STOP
H+
Na+
F
Cl
NH
N
H
O